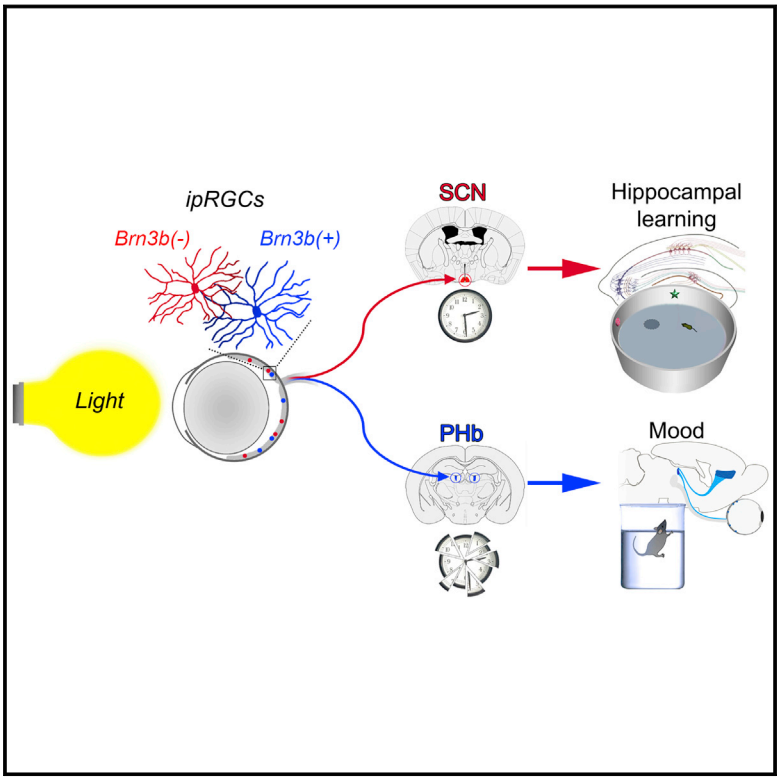
Article

Cell

Light Affects Mood and Learning through Distinct Retina-Brain Pathways

Graphical Abstract



Authors

Diego Carlos Fernandez, P. Michelle Fogerson, Lorenzo Lazzerini Ospri, ..., Haiqing Zhao, David M. Berson, Samer Hattar

Correspondence

diego.fernandez@nih.gov (D.C.F.), samer.hattar@nih.gov (S.H.)

In Brief

The effects of light on learning and mood via intrinsically photosensitive retinal ganglion cells involve a pacemaker-independent role for the suprachiasmatic nucleus as well as distinct circuitry in a region of the thalamus called the perihabenular nucleus.

Highlights

- Distinct ipRGC subpopulations drive the effects of light on learning and mood
- SCN-projecting ipRGCs affect learning without disrupting the central pacemaker
- The ipRGC-PHb pathway drives the light-mediated mood alterations
- Thalamic PHb is integrated in a distinctive circuitry with mood-regulating centers

Fernandez et al., 2018, Cell *175*, 71–84
September 20, 2018 Published by Elsevier Inc.
https://doi.org/10.1016/j.cell.2018.08.004

CellPress

Cell

Light Affects Mood and Learning through Distinct Retina-Brain Pathways

Diego Carlos Fernandez,[1,5,6,*] P. Michelle Fogerson,[2,6] Lorenzo Lazzerini Ospri,[3,6] Michael B. Thomsen,[1,5] Robert M. Layne,[4] Daniel Severin,[3] Jesse Zhan,[1] Joshua H. Singer,[4] Alfredo Kirkwood,[3] Haiqing Zhao,[1] David M. Berson,[2] and Samer Hattar[1,5,7,*]

[1]Department of Biology, Johns Hopkins University, Baltimore, MD 21218, USA
[2]Department of Neuroscience, Brown University, Providence, RI 02912, USA
[3]Department of Neuroscience, Johns Hopkins University, Baltimore, MD 21205, USA
[4]Department of Biology, University of Maryland, College Park, MD 20742, USA
[5]Present address: Section on Light and Circadian Rhythms (SLCR), National Institute of Mental Health, NIH, Bethesda, MD 20892, USA
[6]These authors contributed equally
[7]Lead Contact
*Correspondence: diego.fernandez@nih.gov (D.C.F.), samer.hattar@nih.gov (S.H.)
https://doi.org/10.1016/j.cell.2018.08.004

SUMMARY

Light exerts a range of powerful biological effects beyond image vision, including mood and learning regulation. While the source of photic information affecting mood and cognitive functions is well established, viz. intrinsically photosensitive retinal ganglion cells (ipRGCs), the central mediators are unknown. Here, we reveal that the direct effects of light on learning and mood utilize distinct ipRGC output streams. ipRGCs that project to the suprachiasmatic nucleus (SCN) mediate the effects of light on learning, independently of the SCN's pacemaker function. Mood regulation by light, on the other hand, requires an SCN-independent pathway linking ipRGCs to a previously unrecognized thalamic region, termed perihabenular nucleus (PHb). The PHb is integrated in a distinctive circuitry with mood-regulating centers and is both necessary and sufficient for driving the effects of light on affective behavior. Together, these results provide new insights into the neural basis required for light to influence mood and learning.

INTRODUCTION

The constancy of the solar cycle as a signal for the regulation of mammalian behavior is manifested, among other things, in the powerful effects that light exerts on mood and cognition. These effects have been documented in laboratory animals (Bedrosian et al., 2011; LeGates et al., 2012), as well as in humans (Vandewalle et al., 2010). Depressive symptoms and cognitive dysfunction linked to light can be brought on by natural conditions or by people's own agency by traveling across time zones and experiencing jet lag or in shift-work (Jaeger et al., 2006; Kurlansik and Ibay, 2012; Roh et al., 2016; Scott et al., 1997). The magnitude of these mood effects is large as ~20% of the general population is affected (Melrose, 2015) with symptoms being fairly common, including anhedonia and feelings of helplessness (Russo and Nestler, 2013).

In mammals, light detection occurs exclusively in the retina (Hattar et al., 2003; Wässle, 2004). In addition to classical rod and cone photoreceptors, a subpopulation of retinal ganglion cells (RGCs) that express the photopigment melanopsin (*Opn4*), making them intrinsically photosensitive (ip)RGCs, constitute the third type of photoreceptors (Berson et al., 2002; Hattar et al., 2002; Provencio et al., 2000). At present, 5 subtypes (M1–M5) of ipRGCs have been described (Ecker et al., 2010; Schmidt et al., 2011). Their central projections differ amply, reflecting in this variety the multiform nature of the non-image-forming visual functions they participate in such as circadian photoentrainment and sleep regulation (Altimus et al., 2008; Hattar et al., 2006). A major ipRGC target is the hypothalamic suprachiasmatic nucleus (SCN), which houses a central pacemaker that orchestrates peripheral clocks to drive circadian rhythmic coherence (Morin, 2013). Genetic ablation of ipRGCs completely abrogates light reception at the SCN level, suggesting that ipRGCs constitute the only conduit for light input to modulate circadian brain functions (Güler et al., 2008).

Notably, the regulation of mood and learning by light is also absent in mice where ipRGCs are ablated (LeGates et al., 2012, 2014), indicating that ipRGCs are the main sensory channel driving these behavioral effects. The ipRGC central targets mediating these effects, however, remain unknown. Here, we show that a subset of ipRGCs, that are defined by the lack of Brn3b expression and project to the SCN, are sufficient to drive light-mediated cognitive deficits without disrupting the SCN clockwork machinery. An SCN-independent pathway mediates light-induced mood changes through ipRGC input to the perihabenular nucleus (PHb) of the dorsal thalamus. PHb neurons project to well-characterized mood-regulating centers. Furthermore, the PHb is both necessary and sufficient for driving the effects of light on affective behavior. These findings reveal two distinct retinal-brain pathways that mediate the direct effects of light on mood and cognition.

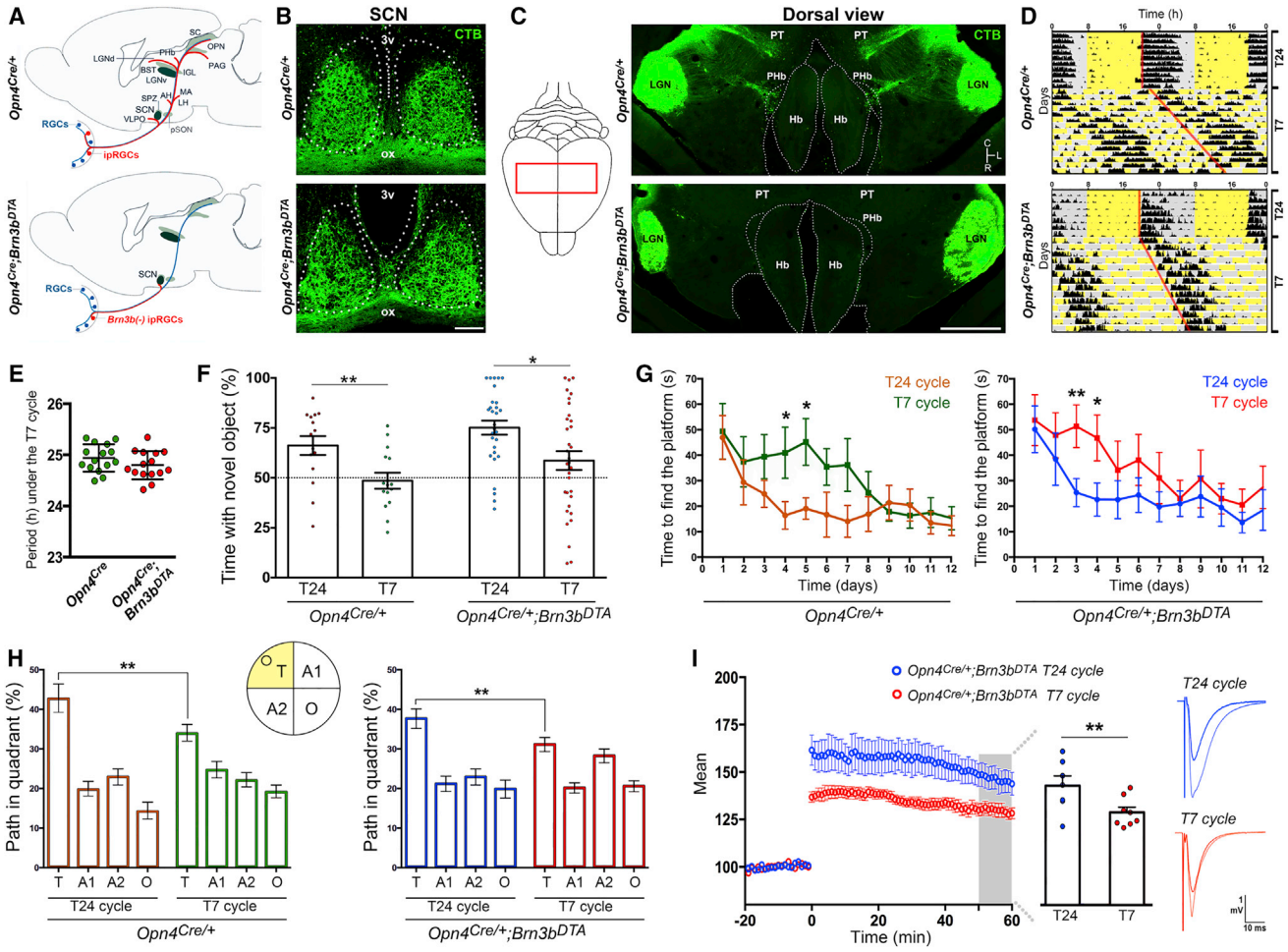


Figure 1. SCN-Projecting ipRGCs Drive Light-Induced Cognitive Deficits

(A) Schemes showing ipRGC projections in *Opn4*$^{Cre/+}$ (control) and *Opn4*$^{Cre/+}$;*Brn3b*^{zDTA} mice.

(B and C) Retinal projections (Brn3b(−) ipRGCs) were retained in the SCN (B), but absent in most ipRGC targets (C) in *Opn4*$^{Cre/+}$;*Brn3b*^{zDTA} mice.

(D and E) The pattern of locomotor activity (D) and circadian periods length (E) under the T7 cycle were similar between groups. Data are mean ± SEM, by Student's t test (n = 15).

(F) A significant reduction in the time exploring the novel object was observed in mice exposed to the T7 cycle versus T24-housed mice. The statistical analysis compared to 50% (dotted lines) was *Opn4*$^{Cre/+}$: T24 $p < 0.01$; T7 $p = 0.716$; *Opn4*$^{Cre/+}$;*Brn3b*^{DTA}: T24 $p < 0.001$; T7 $p = 0.754$; by one sample t test (n = 15–35).

(G and H) Using the MWM, we found significant deficits during learning (G) and test (H) trials in mice exposed to the T7 cycle versus T24-housed mice (n = 12–14).

(I) T7-housed *Opn4*$^{Cre/+}$;*Brn3b*^{DTA} mice showed significant LTP deficits versus T24-housed mice (n = 8–10 mice).

Data are mean ± SEM. *p<0.05, **p<0.01, by Tukey's test. 3v, third ventricle; ox, optic chiasm; LGN, lateral geniculate nucleus; Hb, habenular complex; PT, pretectum. Scale bars, 100 μm (B), 1 mm (C).

See also Figure S1.

RESULTS

The SCN-Projecting ipRGCs Drive the Effects of Light on Learning

The use of an ultradian light cycle (T7 cycle; alternating 3.5-hr periods of light and darkness) allowed us to determine the direct effects of light on mood and learning (LeGates et al., 2012). To investigate whether light input to the SCN is sufficient to drive the behavioral alterations induced by the T7 cycle, we used a previously described mouse line, *Opn4*$^{Cre/+}$;*Brn3b*$^{zDTA/+}$ (Chen et al., 2011), in which Brn3b(−) ipRGCs that innervate the SCN survive, whereas Brn3b(+) ipRGCs projecting outside the SCN are substantially ablated (Figures 1A–1C and S1A–S1C). *Opn4*$^{Cre/+}$;*Brn3b*$^{zDTA/+}$ mice photoentrained under a normal light/dark cycle (T24 cycle), and their circadian periods were lengthened when exposed to the T7 cycle, similar to *Opn4*$^{Cre/+}$ (control) mice (Figures 1D and 1E). Thus, the general circadian responses are intact in these animals.

Under the T24 cycle, *Opn4*$^{Cre/+}$ and *Opn4*$^{Cre/+}$;*Brn3b*$^{zDTA/+}$ mice showed similar learning and cognitive functions (Figures 1F–1H; novel object recognition [NOR] test: $p = 0.57$; Morris water maze [MWM], test trial: $p = 0.5$, by Tukey's test), indicating that the ablation of Brn3b(+) ipRGCs did not affect the cognitive functions of these animals. When exposed to the T7 cycle for

2 weeks, *Opn4*$^{Cre/+}$;*Brn3b*$^{zDTA/+}$ animals displayed cognitive deficits, similar to those observed in T7 cycle-housed control (*Opn4*$^{Cre/+}$) mice (Figures 1F–1H). Specifically, T7 cycle-housed mice spent significantly less time exploring the novel object than mice housed under the T24 cycle (Figures 1F and S1D). In the MWM, T7 cycle-housed mice exhibited significant deficits during training, test, and reverse phases, relative to mice housed under the T24 cycle (Figures 1G, 1H, S1E, and S1F). For both behavioral tests, no significant differences were found in the results obtained from *Opn4*$^{Cre/+}$ and *Opn4*$^{Cre/+}$;*Brn3b*$^{zDTA/+}$ mice exposed to the T7 cycle (Figures 1F–1H; NOR: $p = 0.45$; MWM, test trial: $p = 0.86$; by Tukey's test).

In line with the behavioral studies, hippocampal long-term potentiation (LTP) was significantly attenuated in both *Opn4*$^{Cre/+}$ (control) and *Opn4*$^{Cre/+}$;*Brn3b*$^{zDTA/+}$ mice when housed under the T7 cycle, relative to T24-housed groups (Figures 1I and S1G). The LTP alterations were specific to activity-dependent potentiation by the theta-burst stimulus, because other aspects of transmission were normal (Figures S1H and S1I). Together, these results highlight the sufficiency of the Brn3b(−) ipRGCs in mediating light-induced LTP and cognitive deficits.

The T7 Cycle Alters the Photoresponsiveness of the SCN

We previously found that the rhythmic expression of the clock gene *period2* (PER2) in the SCN was unperturbed by the T7 cycle (LeGates et al., 2012). This raises a conundrum: if the SCN remains responsive to light under the T7 cycle, why are PER2 levels unaffected under a recurring light activation? To address this question, we first tested whether the photic responsiveness of SCN neurons is affected under the T7 cycle, by evaluating the phosphorylation of CREB (cAMP response element-binding protein), one of the first steps in gene induction in response to light (Chawla, 2002). Light-induced pCREB levels were similar in the SCN from animals maintained under T24 and T7 cycles (Figures 2A–2D), indicating that the SCN is still responsive to light in T7 cycle-housed mice. Interestingly, it was recently shown that the SCN can act not only as a circadian pacemaker, but also as a relay for light input to peripheral oscillators (Izumo et al., 2014). To explore the role of the SCN as a light relay versus a circadian pacemaker, we analyzed the effects of T7 cycle on *Period1* (PER1), a clock gene that shows both a robust rhythmic expression and a fast response to light (Travnickova-Bendova et al., 2002). We found that under T7 cycle, the expression levels of PER1 were rhythmic in the SCN (Figures 2E and 2F), whereas the acute effects of light on PER1 induction were abrogated (Figures 2G and 2H). Combined, the effects of light on pCREB levels and PER1 induction indicate that the photic responsiveness of the SCN is distinctively altered by the T7 cycle.

To further investigate the overall changes in SCN photic responsiveness, we performed RNA-sequencing (RNA-seq) on isolated SCN samples (Figure 2A). We found that 29 genes were differentially regulated between T24 and T7 cycle groups (false discovery rate [FDR]-adjusted $p < 0.01$, Figure S2A) including a striking depletion of classical immediate-early genes in T7 cycle-housed animals (Figures 2I and 2J). Gene ontology analysis of differentially regulated transcripts revealed a depletion of genes involved in transcription as well as Ca^{2+} and cAMP responses, further suggesting that the T7 cycle dramatically alters the photic responsiveness of the SCN (Figure S2B). In support of the RNA-seq data, we found a significant decrease in light-mediated c-Fos induction in SCN neurons under the T7 cycle, compared with T24-housed mice (Figures S3A and S3B). c-Fos induction in the SCN requires the phosphorylation of both CREB and ELK-1, leading to the recruitment of CREB-binding protein, resulting in gene transcription through the acetylation and phosphorylation of histones, including histone-3 (H3) (Chawla, 2002; Kako and Ishida, 1998). In contrast to pCREB, the light-induced pELK-1 and pH3 levels were significantly reduced in SCN neurons from animals housed under the T7 cycle (Figures S3A, S3C, and S3D). Combined, these data show that the SCN becomes refractory to light-induced transcriptional changes that would otherwise impinge on the clockwork machinery under the T7 cycle.

The Effects of Light on Mood Are Independent of the SCN

To investigate whether Brn3b(−) SCN-projecting ipRGCs also affect mood-related behaviors, mice were housed under the T24 or T7 cycles, and the sucrose preference test (SPT), tail suspension test (TST), and forced-swim test (FST) were performed. Under normal light conditions, *Opn4*$^{Cre/+}$ (control) and *Opn4*$^{Cre/+}$;*Brn3b*$^{zDTA/+}$ mice showed no significant differences in their behavioral responses (Figure 3; SPT, $p = 0.600$; TST, $p = 0.921$; FST, $p = 0.859$; by Tukey's test). Remarkably, ablating ipRGC projections outside the SCN abolished mood alterations induced by the T7 cycle. Specifically, *Opn4*$^{Cre/+}$;*Brn3b*$^{zDTA/+}$ mice exposed to the T7 cycle showed no significant differences in the sucrose preference index (Figure 3A), immobility time during the TST (Figure 3B) and FST (Figure 3C), compared to mice housed under the T24 cycle. In addition, under the T7 cycle, results obtained from *Opn4*$^{Cre/+}$;*Brn3b*$^{zDTA/+}$ mice were significantly different compared with *Opn4*$^{Cre/+}$ mice (Figure 3; SPT, $p < 0.001$; TST, $p < 0.05$; FST, $p < 0.001$; by Tukey's test). Thus, ipRGC pathways, distinct from the SCN, must be responsible for driving light regulation of mood.

PHb Neurons Receive Direct Input from ipRGCs

Among the ipRGC targets that might mediate the perturbation of affective behavior by unnatural light cycles, a region of the dorsal thalamus, adjacent to the epithalamic lateral habenula (LHb), is of particular interest. This region, which was previously termed perihabenular region (PHb), has been shown to receive retinal innervation (Hattar et al., 2006; Morin and Studholme, 2014). We first evaluated the light-responsiveness of the PHb. Wild-type (WT) mice showed a robust light-mediated c-Fos induction throughout the PHb (Figures 4A and 4C), whereas mice lacking ipRGC innervation to the PHb (*Opn4*$^{Cre/+}$;*Brn3b*$^{zDTA/+}$) showed no induction of c-Fos (Figure S3E). We found that T7-housed WT mice showed a normal c-Fos induction in the PHb after a light pulse exposure (Figures 4B and 4C), suggesting that, contrary to the SCN, the PHb photoresponsiveness is unaltered under T7 cycle.

PHb neurons show a robust rhythmic expression of the clock gene PER2 under normal light conditions (Figure 4D). The c-Fos induction observed in PHb neurons raises the possibility that

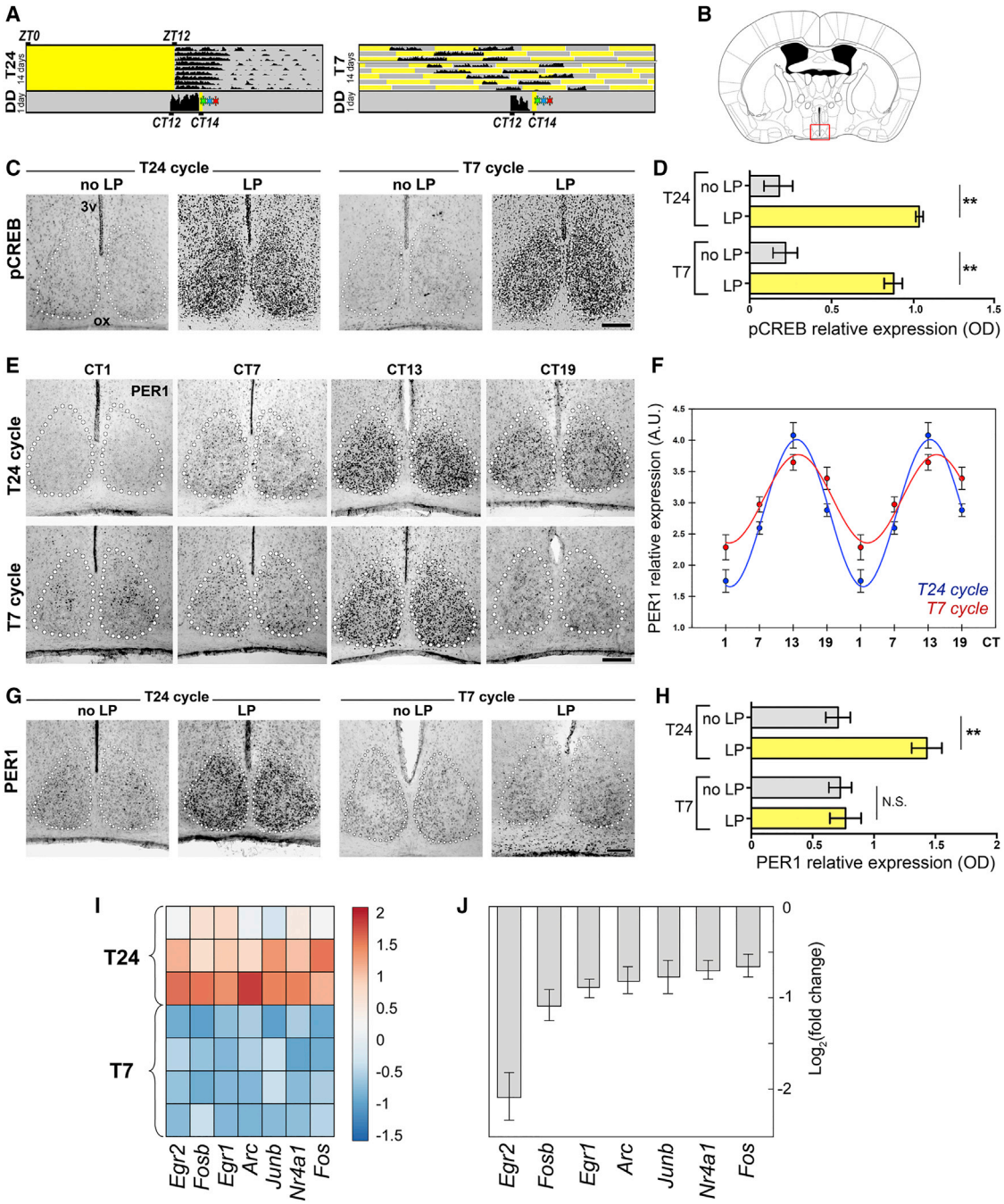


Figure 2. Photic Responsiveness and Gene Expression in the SCN

(A) T24- or T7-housed mice were kept in darkness for 1 day, exposed to a light pulse, and immediately perfused for assess pCREB levels (green star), perfused after 90 min for PER1 levels (red star), or after 60 min for SCN dissections (blue star).

(B) Scheme showing a coronal brain section at SCN level.

(C and D) A significant increase in pCREB levels were observed in both light pulse (LP)-treated groups, versus no light pulse (noLP) controls. Data are mean ± SEM. **p<0.01; by Tukey's test (n = 5–6 mice).

(E and F) No significant differences in the rhythmicity of PER1 levels were observed between groups (F). Data are mean ± SEM; by Student's t test (n = 4–5 mice).

(G and H) The exposure of mice to the T7 cycle affected the light-mediated induction of PER1 in the SCN. Data are mean ± SEM. **p<0.01; by Tukey's test (n = 5–6 mice).

(I) Heatmap of relative gene expression levels for selected immediate-early genes.

(J) Fold change in expression level of immediate-early genes in T7 versus T24 samples (T24: n = 3, T7: n = 4 replicates; SCN tissue was pooled from 3 mice per replicate, FDR-adjusted p < 0.01 for all samples).

3v, third ventricle; ox, optic chiasm; DD, constant darkness; ZT, zeitgeber time. Scale bars, 100 μm.

See also Figures S2 and S3.

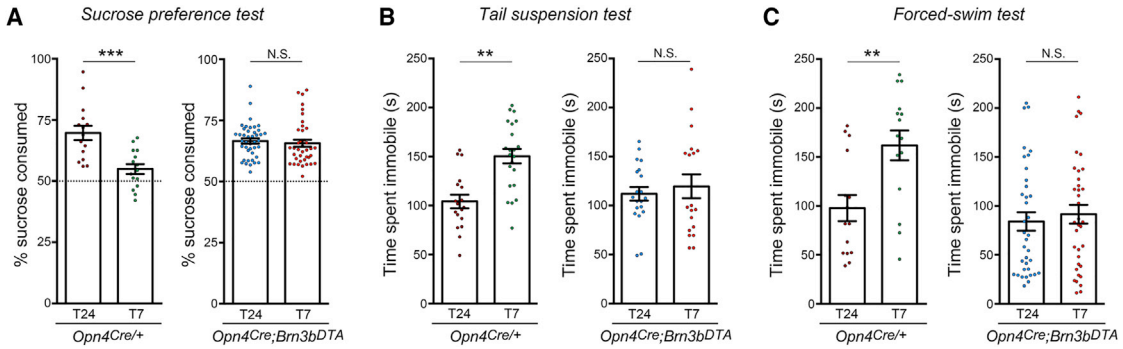


Figure 3. ipRGC-SCN Pathway Is Not Involved In Light-Mediated Mood Alterations

(A–C) *Opn4*$^{Cre/+}$ mice housed under the T7 cycle showed mood alterations, as shown in the SPT (A), TST (B), and FST (C). These mood-related deficits induced by the T7 cycle were abolished in *Opn4*$^{Cre/+}$;*Brn3b*^{zDTA} mice. For the SPT, the total volume consumed (in mL) was *Opn4*$^{Cre/+}$, T24 = 5.3 ± 1.2 and T7 = 5.1 ± 0.8 and *Opn4*$^{Cre/+}$;*Brn3b*^{DTA}, T24 = 5.1 ± 1.1 and T7 = 5.8 ± 0.8 by Tukey's test. In addition, the statistical analysis versus 50% (dotted lines, A) was *Opn4*$^{Cre/+}$, T24 $p < 0.01$ and T7 $p = 0.30$ and *Opn4*$^{Cre/+}$;*Brn3b*^{DTA}, T24 $p < 0.01$ and T7 $p < 0.01$ by one sample t test.

Data are mean ± SEM. ***p<0.001, **p<0.01, by Tukey's test. *Opn4*$^{Cre/+}$ mice, n = 15–16; *Opn4*$^{Cre/+}$;*Brn3b*^{DTA} mice, n = 29–42.

under the T7 cycle, neurons may be abnormally (and chronically) activated by the appearance of light every 3.5 hr, which would lead to alterations in PER2 rhythmic expression. Indeed, when WT mice were housed under the T7 cycle, PER2 rhythmicity was abolished in the PHb, maintaining high PER2 levels throughout (Figure 4D). These results suggest that light input has a direct impact over clock genes expression, as revealed by alterations in PER2, known to show a slow response to light (Travnickova-Bendova et al., 2002; Wilsbacher et al., 2002). To further evaluate whether ipRGCs are involved in this process, we tested mice in which ipRGCs are ablated by the expression of the attenuated diphtheria toxin (*Opn4*$^{aDTA/aDTA}$). We previously found a drastic reduction of ipRGC innervation in these animals at 6 months of age (Ecker et al., 2010; Güler et al., 2008; LeGates et al., 2012). Specifically, only sparse retinal fibers were observed in the most caudal PHb region in *Opn4*$^{aDTA/aDTA}$ mice (Figures S4A and S4B). Importantly, in the absence of the ipRGC projections, PER2 rhythmicity in the PHb was maintained in *Opn4*$^{aDTA/aDTA}$ mice housed under the T7 cycle (Figures 4E, S4C, and S4D). These findings reveal that irregular light/dark cycles perturb the circadian clock machinery selectively in the PHb through an ipRGC-dependent circuit.

Retinal innervation to the PHb was precisely mapped using intravitreal injections of the tracer cholera toxin β-subunit (CTβ). Retinal axons labeled a wedge-shaped zone near the boundary between the dorsal thalamus and the LHb, especially caudally, in regions typically included in the central lateral (CL) or the lateral posterior (LP) thalamic nuclei (Figures 4F and S4A). A few retinal fibers penetrate into the most lateral edge of the LHb (Figure S4A). The retina-PHb circuit was further characterized by mapping the presynaptic terminals of ipRGC axons by using *Opn4*$^{CreERT/+}$;*ROSA*$^{Synaptophysin\text{-}tdTomato}$ mice (Figure S4E). Labeled puncta, marking ipRGC output synapses, were densely distributed throughout the PHb (Figures 4G and S4F). To determine the identity of the RGCs that project to this area, we injected the tracer CTβ into the PHb in WT mice (Figure 4H). In the contralateral retina, all retrolabeled RGCs (70.6 ± 5.2 cells/retina, n = 4 mice) were melanopsin immunopositive (Figures 4I and 4J). Thus, the PHb receives its retinal input exclusively from ipRGCs.

Next, we sought functional evidence for retinal influence on PHb neurons. For that, we expressed channelrhodopsin-2 (ChR2) in retinal axons by intravitreal injections of an AAV2/ChR2-EYFP (Figures 4K, S4G, and S4H). PHb cells recorded in current clamp exhibited bursting responses when relatively hyperpolarized (−70 mV), whereas a tonic mode of firing was observed when cells were relatively depolarized (−60 mV) (Figures S4I and S4J), similar to previous descriptions of thalamic neurons (Kim et al., 2001; Sherman, 2001), and a subpopulation of LHb neurons (Wagner et al., 2017). Activation of local ChR2-positive retinal axons by flashes of blue light (2 ms) evoked cationic excitatory postsynaptic currents (EPSCs) in a subset (9.5%, n = 63 cells) of patch-recorded PHb neurons (Figures 4L, 4M, and S4K–S4M). Together, these data indicate that ipRGCs provide excitatory synaptic input to PHb neurons.

PHb Is a Distinct Thalamic Region that Projects to Mood-Regulating Centers

The location of the PHb was delineated using markers of gene expression exclusively associated with thalamic or epithalamic areas. For that, the PHb area was outlined based on the light-mediated c-Fos induction. We found that most c-Fos(+) cells were co-labeled with GRID2IP (Figure 5A), a marker for dorsal thalamic nuclei (Nagalski et al., 2016). Only a minor fraction of total PHb c-Fos(+) cells co-localized with Brn3a (also known as POU4F1, Figure 5B), a marker for the epithalamic LHb (Quina et al., 2015). Additionally, we observed that most ipRGC terminals were in close apposition with thalamic neurons immunopositive for GRID2IP or PKCd (Figures S5A and S5B), another marker used for delineating the dorsal thalamus (Nagalski et al., 2016). In sum, these results assign the PHb as part of the dorsal thalamus.

We then investigated the PHb downstream circuitry using CTβ injections to uncover targets potentially implicated in mood regulation. We found that the most prominently labeled region was the ventral medial prefrontal cortex (vmPFC) (Figure S5C).

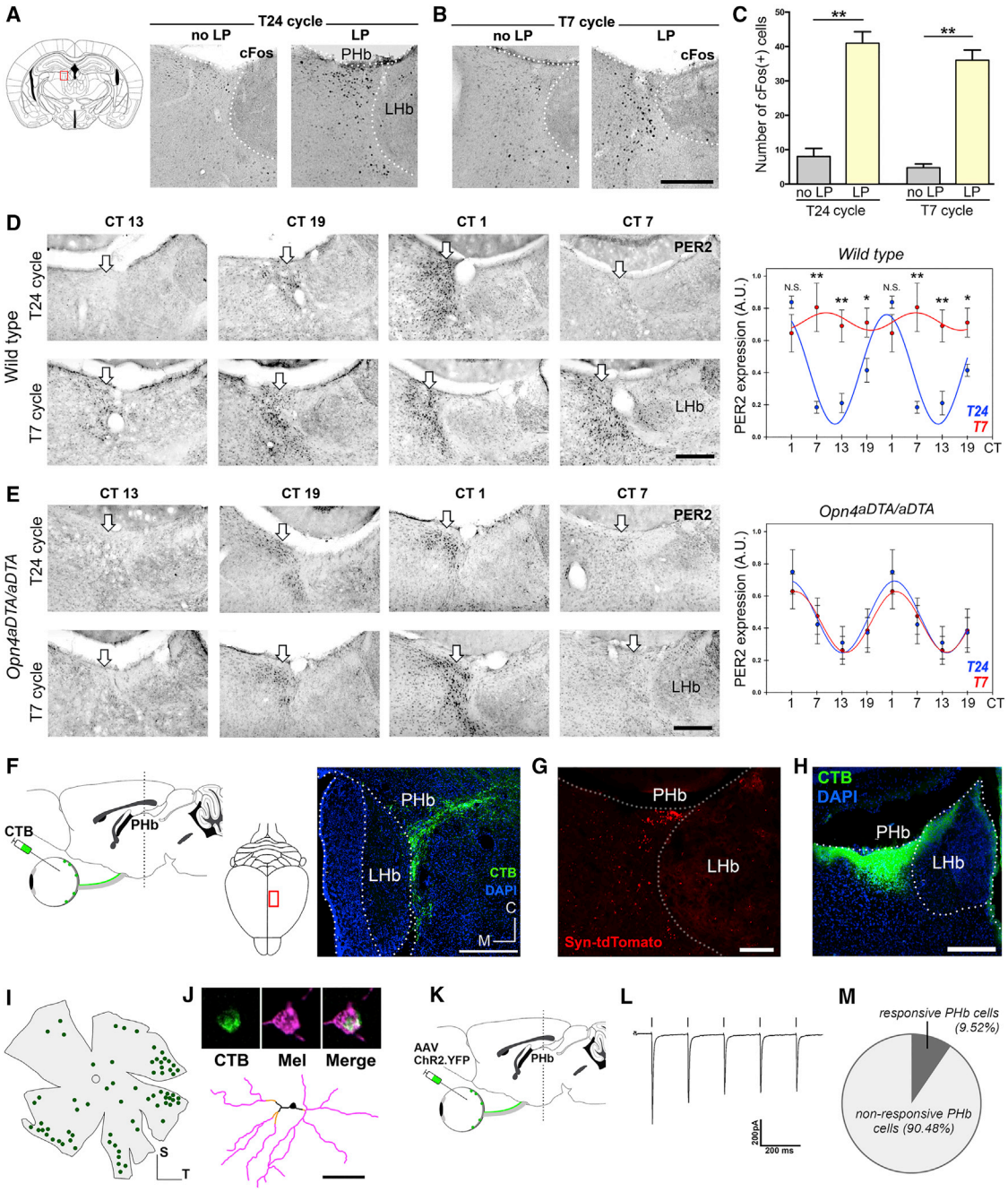


Figure 4. Characterization of Retinal Input to the PHb

(A–C) A significant increase in the number of light-induced c-Fos(+) cells in PHb were observed in both groups, versus no light pulse controls. Data are mean ± SEM. **p<0.01; by Tukey's test (n = 5 mice).

(D and E) Immunohistochemical evidence for the rhythmic PER2 expression in the PHb (white arrows) in mice housed under the T24 or T7 cycles. In WT mice, PER2 levels exhibited circadian rhythmicity in the PHb under the T24 cycle, but the T7 cycle exposure significantly raised PER2 expression levels (D). In mice lacking ipRGC projections (*Opn4*$^{aDTA/aDTA}$), PER2 rhythms in the PHb (E) became impervious to the effects of the T7 cycle. Data are mean ± SEM. *p < 0.05, **p < 0.01, by Student's t test (n = 4–5 mice).

(F) Retinal projections to the PHb traced by CTβ.

(G) ipRGC afferents to PHb contain a synaptophysin fusion protein (*Opn4*^{CreERT};*ROSA*$^{Syn\text{-}tdTomato}$).

(H–J) CTβ was stereotaxically injected in the PHb (H), and all retrolabeled RGCs (I) were melanopsin(+) (J). From a total of 49 ipRGCs analyzed, 46 cells were identified as M1 and 3 were M3 (n = 8 mice).

(legend continued on next page)

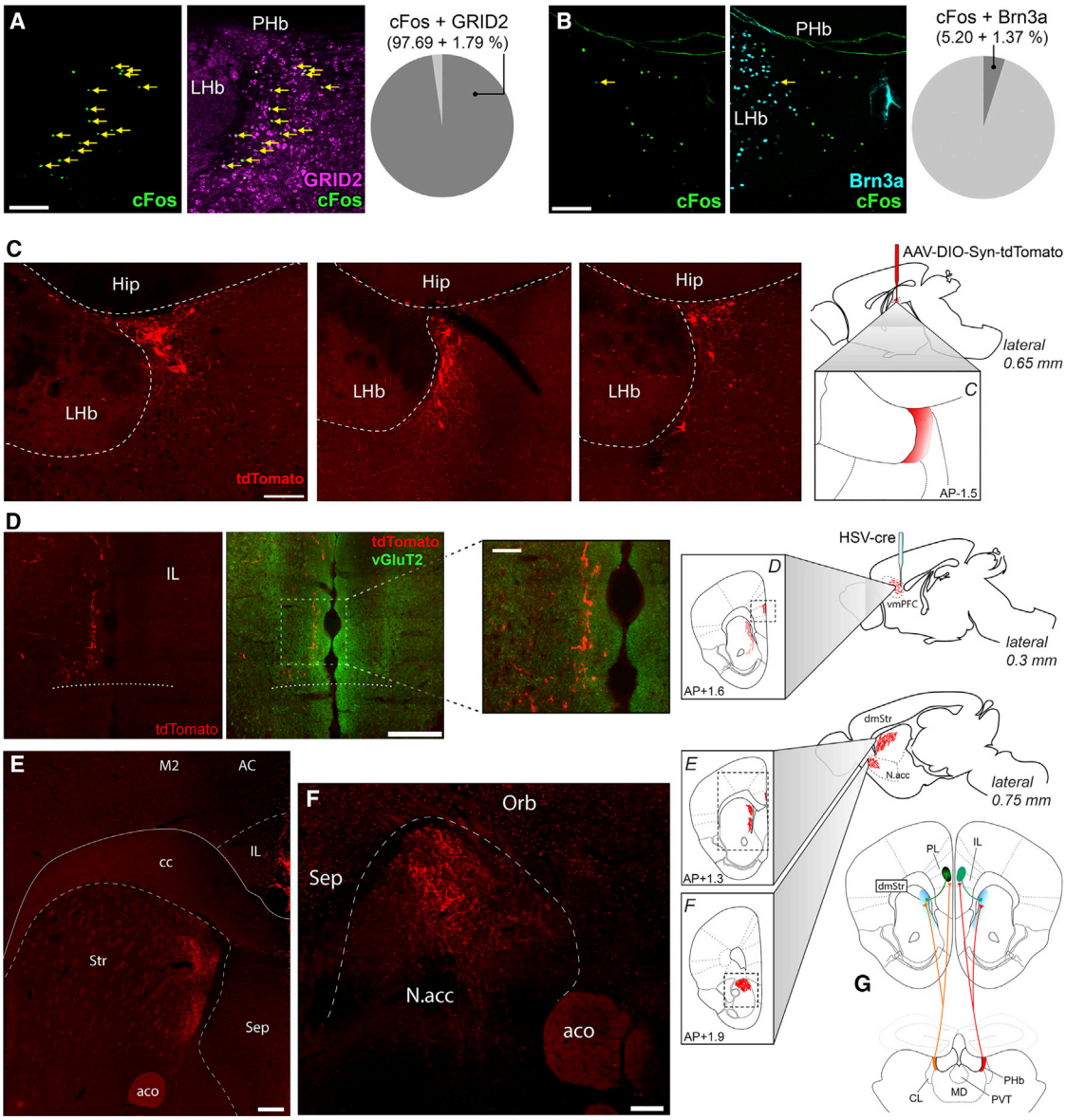


Figure 5. Thalamic PHb Projects to Mood-Regulating Centers

(A and B) Light induced cFos(+) cells in the PHb were colocalized with GRID2 (A) or Brn3a (B) markers. Data are mean ± SEM (n = 3 mice).

(C–F) HSV/cre was injected into the vmPFC, while AAV/DIO-synaptophysin-tdTomato was injected into the PHb. Labeled somas were exclusively found in the PHb (C). PHb neurons have three targets: the vmPFC, including the IL (D), the dorsomedial striatum (E), and the NAc (F) (n = 12 mice).

(G) These experiments revealed a thalamocortical loop, represented here diagrammatically.

cc, corpus callosum; M2, secondary motor cortex; AC, anterior cingulate cortex; Str, striatum; aco, anterior commissure; Sep, septal nuclei; Orb, orbitofrontal cortex, Hip, hippocampus. Scale bars, 50 μm (D, inset); 100 μm (A–C); 200 μm (D–F).

See also Figure S5.

In particular, there were retrogradely labeled somas in layers V and VI of the infralimbic (IL) and prelimbic (PL) cortices bilaterally with respect to injection site and anterograde-labeled fibers in layers I and III-IV of the IL ipsilaterally. This result pointed to the existence of a thalamocortical loop between the PHb and vmPFC that is distinct from the CL or the LP nuclei, which are

(K–M) Optogenetic evidence for functional connections between ipRGCs and PHb neurons (K). Current response in a representative PHb neuron is shown (L). A subpopulation of PHb neurons showed a ChR2-induced response to light pulses (M) (n = 63 cells).

3v, third ventricle; ox, optic chiasm; no LP, no light pulse; LP, light pulse. Scale bars, 100 μm (J); 200 μm (B and D–H).

See also Figures S3 and S4.

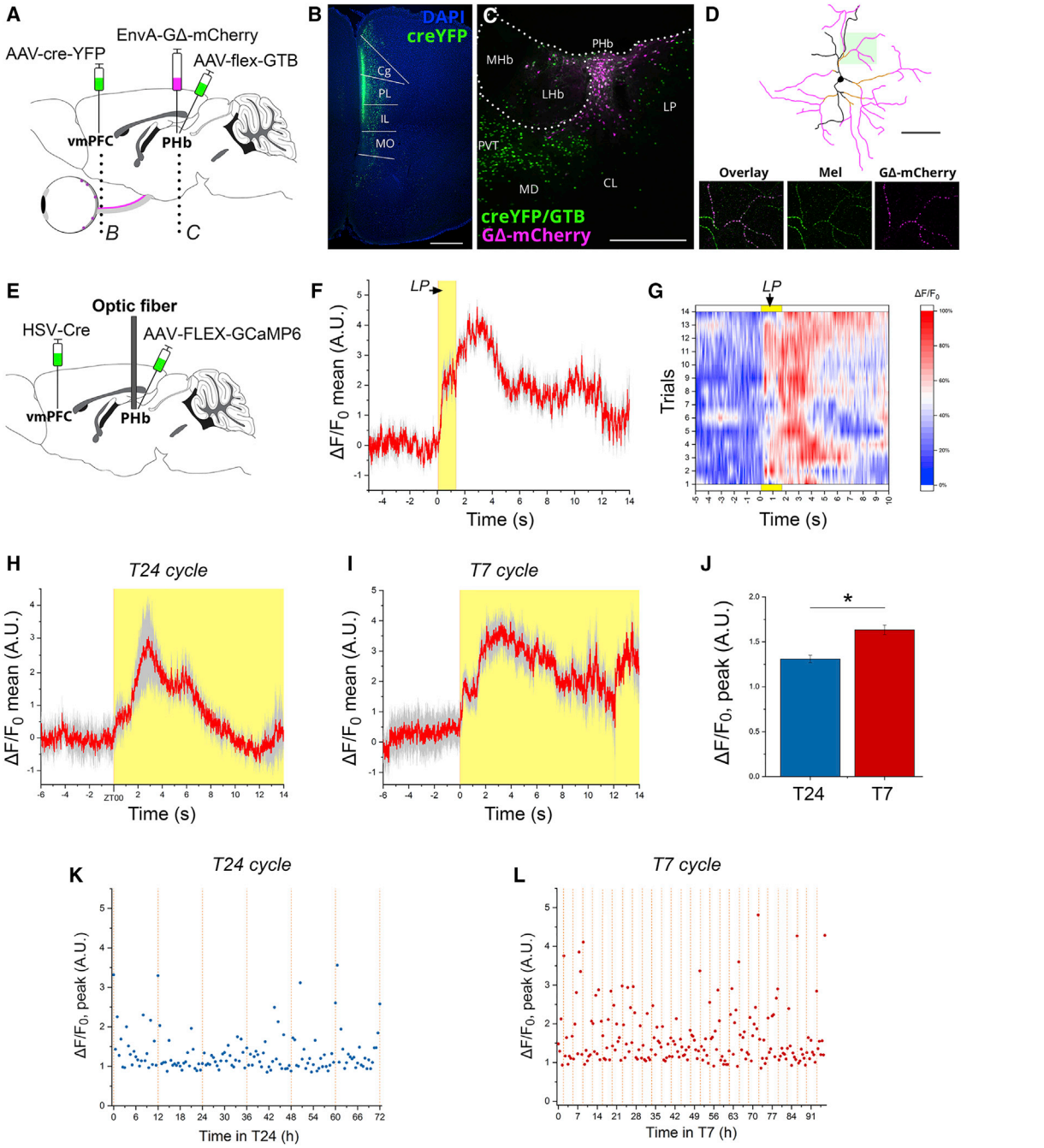


Figure 6. Disynaptic Circuits Connect ipRGCs to Mood-Regulating Centers

(A–D) A three-virus retrograde transynaptic tracing system was used to identify the retino-PHb-vmPFC pathway (A). Injection sites were confirmed in the vmPFC (B) and PHb (C). EnvA-GΔRabies-mCherry expresses mCherry in PHb neurons expressing both Cre-EYFP and the Cre-dependent helper AAV (starter neurons) and presynaptic inputs to these neurons. A retrolabeled RGC expressing mCherry counterstained for melanopsin is shown (D).

(E) The PHb was transfected with a fluorescent Ca^{2+} sensor by injecting a cre-dependent GCaMP6m vector in the PHb region and a retrogradely transported cre virus in the vmPFC.

(F) Average response to a 2-s light pulse delivered at zeitgeber time (ZT) 18 to a mouse kept under the T24 cycle. The Ca^{2+} transient comprises a fast-rising component plateauing for 1.1 s before a second phase supervenes to generate a higher peak 3 s after light presentation. A biphasic response could bespeak either the transfection in our experimental design of two distinct (sub)populations that respond to light with different time courses or a functional property of a single neuronal population.

(G) A map of the 14 individual trials averaged in (F) is shown.

(H) PHb activity following regularly scheduled lights-on event in T24 cycle.

(legend continued on next page)

not known to project to the vmPFC (Noseda et al., 2010; Voorn et al., 2004). To increase the precision of our projection tracing, we used a dual injection strategy with a retrogradely transported Cre-carrying vector injected in the IL and a *Cre*-dependent vector carrying synaptophysin-tdTomato injected in the PHb (Figures 5C and 5D). We found that one of the PHb targets is indeed the vmPFC (Figure 5D). To determine which vmPFC subdivisions are innervated, we used vGluT2 staining to reveal the ventral boundary of the cortex (Figure S5D). PHb terminals extended ventrally within 200 μm of the ventral cortical boundary (Figure 5D), which is assigned IL territory. Furthermore, PHb terminals revealed a compression of cortical layers characteristic of the cytoarchitecture of IL. Based on the same factors, the most dorsal extent of the PHb's cortical innervation field may fall within the ventral PL. The second and third targets of PHb neurons are the dorsomedial striatum (Figure 5E) and the nucleus accumbens (NAc) (Figure 5F). It should be noted that the dorsomedial striatum also receives input from the same cortical areas targeted by the PHb, indicating that PHb is part of a thalamo-frontocortico-striatal loop (Figures 5G, S5E, and S5F). Finally, we noticed that a subset of labeled PHb neurons appear to send collaterals into the lateral part of the LHb (Figure S5G). Control injections of HSV-cre in the dorsomedial prefrontal cortex did not result in any labeled cells in the PHb proper (Figure S5H). Together, these results demonstrate that the PHb is incorporated into a loop reminiscent of limbic thalamic nuclei (Vertes et al., 2015). As a cohesive neuronal cluster with distinctive connectivity, genetic, and functional properties (including being a circadian oscillator), the PHb must be properly reckoned as an independent, previously unrecognized thalamic nucleus.

Disynaptic Circuits Connect ipRGCs to Specific Mood-Regulating Regions

To determine whether the PHb links ipRGCs to vmPFC through a disynaptic circuit, we used a triple-virus *trans*-synaptic retrograde tracing strategy (Schwarz et al., 2015): a retrogradely transported AAV/Cre-YFP was injected into the vmPFC (Figures 6A and 6B). Then, presynaptic partners of these thalamocortical relay neurons were labeled transynaptically by injecting a *Cre*-dependent helper virus followed by EnvA-pseudotyped gΔRabies-mCherry in the PHb (Figure 6C). Finally, labeled PHb-projecting RGCs were found, and all of them were melanopsin(+) (Figure 6D). Using this strategy, we labeled from one to seven ipRGCs per animal; the low number of labeled ipRGCs could be due to the low probability requirement for the three viruses to infect the same cells in the PHb. Therefore, we also deployed a dual-virus strategy: a retrograde helper virus was injected into the vmPFC, followed by EnvA-pseudotyped G-deleted rabies injected into the PHb (Figures S6A–S6D). Using this strategy, 25 ± 7.1 labeled ipRGCs were found per retina. In sum, these results confirm the existence of a disynaptic pathway linking ipRGCs through PHb to vmPFC.

Next, we sought to characterize the physiology of the PHb *in vivo*. The target cell population was transfected with a fluorescent Ca^{2+} indicator, GCaMP6m, by injections of a cre-dependent vector in the PHb and a retrogradely transported cre-carrying vector in the vmPFC; an optical fiber was implanted above the PHb to deliver and collect light locally in awake, free-moving mice (Figure 6E). We first confirmed that vmPFC-projecting PHb neurons responded to brief light pulses delivered in the active phase of mice (Figure 6F) with a biphasic Ca^{2+} transient characterized by a fast component rising 90 ± 3 ms after external light presentation and by a subsequent slower further rise peaking 3 s thereafter. Return to the pre-stimulus baseline occurs with high temporal variability and irrespective of continued environmental illumination (Figure 6G). To analyze the PHb physiology over longer time-spans, we exposed injected mice to the T24 or T7 cycles, and the PHb activity was recorded. Under both lighting conditions, we observed a fast response of PHb neurons to each dark-light transition (Figures 6H and 6I). A comparison of the magnitude of the peak fluorescence in the PHb in the course of exposure to the two light cycles revealed a significant increase of such activity under the T7 cycle (Figures 6J–6L). In sum, these results indicate that light input modulates the Ca^{2+} dynamics of vmPFC-projecting PHb neurons *in vivo*, with the T7 cycle specifically shown to increase activity.

Chronic Activation of PHb Neurons Is Sufficient to Regulate Mood

The PHb is well positioned to link environmental lighting to affective behavior. If the PHb is required for the effects of light on mood, then chronic activation of the PHb should induce mood disorders in animals housed in a normal light/dark cycle, whereas silencing PHb neurons should block the dysphoric effects induced by the unnatural light cycle. To achieve long-lasting activation of light-responsive PHb neurons, we used a chemogenetic strategy based on designer receptors exclusively activated by designer drugs (DREADDs) (Roth, 2016) combined with *c-Fos*^{CreERT2} mice. A *Cre*-dependent AAV encoding an excitatory (Gq) was bilaterally injected in the PHb (Figure 7A). One week later, mice received a light pulse (circadian time [CT] 14), leading to the expression of the tamoxifen (Tam)-sensitive *Cre* recombinase only in light-responsive neurons. At the end of the light pulse, mice were injected with 4-OH-Tam. Injection sites were invariably restricted to PHb and immediately adjacent thalamic nuclei (Figures 7A and S6E). In AAV-injected *c-Fos*^{CreERT2} mice that received 4-OH-Tam, but without light pulse exposure, only sparse mCherry(+) cells or no detectable mCherry expression was observed in the PHb (Figure S6F). As a control group, littermate *Cre*-negative mice received the

(I) In T7 cycle, the PHb responds to dark-to-light transitions with a biphasic Ca^{2+} transient analogous to the one observed in T24 cycle.
(J) Comparison of peak fluorescence in T24- versus T7-housed mice recorded over 72 hr. Peak fluorescence in T7 cycle is significantly higher (**$p < 0.001$; by Student's t test).
(K and L) Time course of peak fluorescence (calculated as the difference between maximum and median for each sample recording) recorded over multiple days in T24 (K) or T7 (L) cycles. Dashed orange lines indicate light transitions.
Data are mean ± SEM (n = 3 mice). Scale bars, 100 μm (D); 200 μm (C); 500 μm (B).
See also Figure S6.

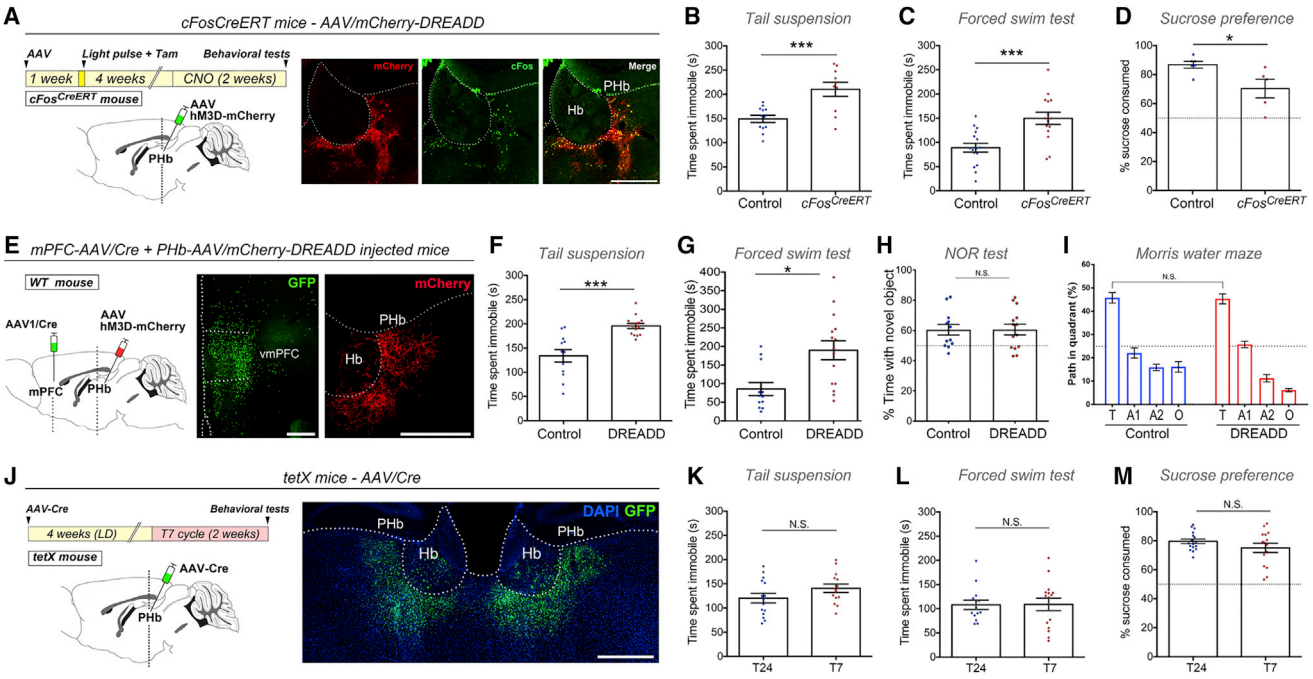


Figure 7. Manipulation of PHb Neuronal Function Alters Affective Behavior

(A) *c-Fos*$^{CreERT/+}$ mice injected with an AAV5/DIO-hM3D-mCherry in the PHb received a light pulse and 4-OH-Tam. Injection sites were evaluated for mCherry, and c-Fos staining was used to confirm CNO-neuronal activation.

(B and C) Chronic activation of light-responsive PHb neurons leads to behavioral alterations, as shown in the TST (B) and FST (C) (n = 10–16).

(D) The SPT was evaluated in *c-Fos*$^{CreERT/+}$ and control-injected mice that received CNO twice a day (see STAR Methods). *c-Fos*$^{CreERT/+}$-injected mice displayed a significant reduced preference for sucrose versus control group (n = 5–7).

(E) vmPFC-projecting PHb cells were chronically activated in mice that were bilaterally injected in the vmPFC with a retrogradely transported AAV/Cre (J and K) and an AAV5/DIO-hM3D-mCherry in PHb.

(F and G) CNO treatment in DREADD-injected mice caused a significant increased in the immobility time in the TST (F) and FST (G) versus control mice (n = 12–15).

(H and I) CNO treatment in DREADD-injected mice had no effect on cognitive functions. For the NOR test (H), the statistical analysis versus 50% (dotted lines) was Control, $p < 0.05$ and DREADD, $p < 0.05$ by one sample t test. Using the MWM test, we found no significant deficits during the test (I) trial (n = 12–14).

(J) AAV5/Cre-GFP was bilaterally injected into the PHb of mice that express tetanus toxin (tetX) in a *Cre*-dependent manner. GFP expression confirms injection site that included the PHb and was largely restricted to immediately adjoining thalamic nuclei.

(K–M) Suppressing PHb synaptic output eliminated any statistical difference in the TST (K), FST (L), and SPT (M) between mice housed under the T24 or T7 cycles. For the SPT, the statistical analysis compared to 50% (dotted lines, M) was: T24 $p < 0.001$ and T7 $p < 0.001$ by one sample t test (n = 14–15).

Data are mean ± SEM. *p< 0.05; ***p<0.001 by Student's t test. Hb, habenular complex. Scale bars, 200 μm.

See also Figures S6 and S7.

same treatment and viral injections. Beginning 4 weeks post-Tam injections, mice continuously received the designer ligand clozapine-N-oxide (CNO) in their drinking water to selectively and tonically activate neurons expressing the designer receptor (hM3D) (Figures S6G–S6I). After 2 weeks of chronic CNO treatment, virally injected *c-Fos*^{CreERT} mice displayed mood alterations, spending significantly more time immobile in both the TST and FST, compared with control mice (Figures 7B and 7C). The SPT was not evaluated in this case out of concern that CNO treatment could affect water palatability. To avoid issues with palatability, in a different set of experiments, AAV-injected *c-Fos*^{CreERT} and *Cre*-negative mice received two (intraperitoneal [i.p.]) injections of CNO (1 mg/kg) per day, during 2 weeks. We found that this CNO treatment induced a significant reduction in the sucrose preference index in *c-Fos*^{CreERT}-injected mice, compared to the control group (Figures 7D and S6J).

To determine whether the PHb-vmPFC circuit is sufficient for driving mood alterations, we performed a long-lasting activation of vmPFC-projecting PHb neurons. WT mice were injected with a retrograde transported AAV/Cre into the vmPFC, and a *Cre*-dependent AAV encoding excitatory(Gq)-mCherry was injected in the PHb (Figure 7E). As a result, mCherry(+) neurons were restricted exclusively to the PHb (Figures 7E and S7A). Control mice received the same treatment, except that an AAV1/GFP was injected in the vmPFC. Four weeks after injections, mice kept in T24 cycle (Figure S7B) received CNO in their drinking water for 2 weeks, as described above. Chronic activation of vmPFC-projecting PHb neurons induced significant alterations in mood, as evaluated using the TST and the FST (Figures 7F and 7G).

We then investigated whether the chronic activation of DREADD-controlled PHb neurons could also cause cognitive deficits. Using the same protocol of chronic activation of

mPFC-projecting PHb neurons, we found that the CNO treatment has no significant effect on learning and cognitive functions (Figures 7H and 7I). In the NOR test, both control and DREADD-controlled mice spent significantly more time exploring the novel object (Figures 7H and S7C). During the MWM, both group of mice displayed similar responses during the training and test phases (Figures 7I and S7D). In sum, these results suggest that the PHb is specific for driving the effects of light on mood.

PHb Neurons Are Necessary for the Effects of Light on Mood

We next evaluated whether the PHb is necessary for the mood alterations induced by the unnatural light cycle by inhibiting synaptic release specifically from PHb neurons. Tetanus toxin light chain subunit (tetX) was expressed in PHb neurons by injecting an AAV/Cre-GFP in mice that express tetX in a *Cre*-dependent manner (*R26*$^{tetX\text{-}Z/EG}$) (Zhang et al., 2008) (Figure 7J). Injection sites were confirmed post hoc by assessing GFP expression (Figures 7J and S7E). Four weeks after AAV injections, mice were housed in either T24 or T7 cycles for 2 weeks (Figure S7F). Remarkably, expressing tetX in PHb neurons prevented the T7 cycle-induced mood alterations as tetX-AAV-injected mice housed under the T7 cycle were statistically indistinguishable from those housed under the T24 cycle on the TST, FST, and SPT (Figures 7K–7M and S7G). These results demonstrate that inhibiting PHb neurons blocks the mood alterations triggered by abnormal light cycles.

Next, we explore whether the PHb is specific in mediating the effects of light on mood or whether it is also activated by non-light-dependent treatments that induce mood changes. For that, WT mice were exposed to three different paradigms known to cause mood changes in rodents (see STAR Methods), and the induction of c-Fos was evaluated in PHb neurons, as well as in other brain regions known to be involved in mood control (Choi et al., 2013; Huang et al., 2004; Matsuda et al., 1996). For all the paradigms used, a significant increase in the number of c-Fos(+) cells were found in the LHb and prefrontal cortex, compared with control mice (Figures S7H and S7I), confirming the effectiveness of the paradigms used. However, these same stimuli did not cause a significant induction of c-Fos in PHb neurons. This is in distinct contrast to the robust c-Fos induction mediated by light (Figure S7J). Therefore, the PHb nucleus is part of a circuitry that specifically routes photic stimuli to influence mood.

DISCUSSION

We have previously uncovered that ipRGCs are the sole retinal conduit responsible for signaling light information to modulate mood and cognitive functions (LeGates et al., 2012). Here, we reveal that (1) distinct ipRGC subpopulations drive the effects of light on learning and mood, (2) Brn3b(−) SCN-projecting ipRGCs relay light information to influence cognitive functions without disrupting the central pacemaker, and (3) the thalamic PHb mediates the ipRGC-driven effects of light on mood. Together, these results delineate two distinct retina-brain pathways that mediate the effects of light on learning and mood.

Light Routed through SCN-Projecting ipRGCs Affects Cognitive Functions

The use of the *Opn4*$^{Cre/+}$;*Brn3b*^{zDTA} mouse line allowed us to implicate the ipRGC-SCN pathway in driving the effects of light on learning and memory, which is consistent with previous reports showing that a functional SCN is required for hippocampal learning (Fernandez et al., 2014; Ruby et al., 2008). This animal model, however, still retains minor ipRGC innervation to other brain regions, including the intergeniculate leaflet (IGL). This minor innervation is most likely arising from collaterals of the ~200 SCN-projecting ipRGCs (Fernandez et al., 2016) that remain in the *Opn4*$^{Cre/+}$;*Brn3b*^{zDTA} mice. It is possible that these minor innervations to the non-SCN targets could somehow contribute to the learning deficits observed in mice housed under the T7 cycle. However, based on the previous literature (Fernandez et al., 2014; Ruby et al., 2008) and the substantial innervation to the SCN, the most parsimonious explanation is that the SCN is the main driver of the effects of light on learning and memory.

Recent evidence showed that the SCN can act as a relay for light input to peripheral oscillators, even in the absence of a functional molecular clockwork machinery (Izumo et al., 2014). We found that the SCN remains responsive to light under the T7 cycle, as observed with the robust phosphorylation of CREB, solidifying the role of the SCN as a relay for light input. Additionally, we observed that SCN neurons become refractory to light-induced transcriptional changes, as suggested by the reduced levels of the immediate-early genes, including c-Fos and the light-responsive clock gene, PER1. Light-induction of c-Fos and PER1 depends on two regulatory regions: CRE and SRE, through pCREB and pELK-1 binding, respectively (Chawla, 2002; Coogan and Piggins, 2003). Our results show that under the T7 cycle, the transcription factor ELK-1 is not phosphorylated in response to light, whereas the phosphorylation of CREB was unaffected. This result suggests that CREB and ELK-1 activation pathways are differentially affected by the T7 cycle, consistent with published reports indicating that different intracellular cascades cause phosphorylation of these activators (Coogan and Piggins, 2003; Xia et al., 1996).

The Thalamic PHb Is a Relay for Light-Mediated Mood Control

ipRGCs show widespread projections throughout the brain, including areas controlling sleep and general activity, as well as limbic regions (Hattar et al., 2006). A principal target of ipRGCs revealed in this study is an area of the dorsal thalamus, the PHb, which expresses a circadian clock and shows distinctive connectivity. Our results indicate that the PHb constitutes a distinct thalamic region, with a different pattern of projections compared with the thalamic nuclei into which it has heretofore been subsumed. Specifically, the CL is connected to premotor frontocortical regions and to the dorsolateral striatum, (Voorn et al., 2004), and the thalamic LP nucleus projects to a diverse array of sensory and motor cortices (Noseda et al., 2010). We revealed that PHb neurons send collateral projections to vmPFC, dorsal, and ventral striatum. Prefrontal cortex is fundamental to mood regulation and has been consistently implicated in major depressive disorders (MDD) by imaging studies of patients (Frodl et al., 2009; Meng et al., 2014; Shen et al., 2017) and using animal

models of mood disorders (Shrestha et al., 2015). Another target of PHb, the dorsomedial striatum, is integrated in a thalamo-frontocortical loop, which may be involved in affective-emotional processing. Reduced caudate and putamen volumes were described in MDD patients (Kerestes et al., 2014). The third target of PHb neurons is the ventral striatum, particularly the NAc, which has been extensively implicated in mood control and depression (Francis and Lobo, 2017). In sum, our results provide evidence for a previously unrecognized thalamic nucleus, the PHb, which is both necessary and sufficient for relaying the effects of light on mood.

Perspective

The retino-PHb pathway presented here can satisfactorily account for mood changes wrought by light and represents, therefore, a new general mechanism for mood regulation (Lazzerini Ospri et al., 2017; LeGates et al., 2014). Irregular light stimulation leads to mood alterations associated with changes in the thalamic PHb, including increased activity of PHb neurons, sustained light-mediated induction of the immediate-early gene c-Fos, and a breakdown of clock gene rhythmicity. We speculate that in humans, chronic exposure to light at night could cause similar neuronal changes leading to mood deficits, highlighting the negative impact of irregular light stimulation during the normal day/night cycle. This occurs in a context of lamentable stagnation in the development of effective treatments for mood disorders. While promising drug candidates currently undergoing trials exist, the sad truth is that no radically new class of antidepressants has reached the clinic since the introduction of selective serotonin reuptake inhibitors (SSRIs) in the 1980s (Hillhouse and Porter, 2015).

Reduced cognitive functions have been extensively reported in patients suffering from MDD (Hammar and Ardal, 2009; Jaeger et al., 2006; Roh et al., 2016). Although a direct causal link is missing, current theories suggest that neuroanatomical changes in MDD patients may be the cause of cognitive deficits (Davidson et al., 2002). Our results demonstrate that anatomically distinct neuronal circuits are involved in different light-mediated behavioral deficits and suggest that learning and mood deficits are affected independently. Understanding the neuronal basis for mood and learning regulation by light constitutes a promising step toward new treatments for neuropsychiatric disorders.

STAR★METHODS

Detailed methods are provided in the online version of this paper and include the following:

- KEY RESOURCES TABLE
- CONTACT FOR REAGENT AND RESOURCE SHARING
- EXPERIMENTAL DESIGN AND SUBJECT DETAILS
  - Animals
  - Rhythmic activity measurement
  - Chronic control of PHb function
  - Behavioral test
  - Light-independent paradigms of mood alterations
- METHOD DETAILS
  - Light-mediated gene induction/ protein phosphorylation
  - PER1/2 rhythmic expression
  - Immunofluorescence
  - SCN dissection and RNA-sequencing
  - Retinal injections
  - Stereotaxic injections
  - Electrophysiology
  - Hippocampal recordings
  - Fiber Photometry
- QUANTIFICATION AND STATISTICAL ANALYSIS
  - Morphometric analysis
  - Statistical Analysis
- DATA AND SOFTWARE AVAILABILITY

SUPPLEMENTAL INFORMATION

Supplemental Information includes seven figures and can be found with this article online at https://doi.org/10.1016/j.cell.2018.08.004.

ACKNOWLEDGMENTS

We would like to thank the Johns Hopkins Biology Mouse Tri-Lab—especially Dr. Rejji Kuruvilla—for support and discussion; the Department of Biology at the University of Maryland and Dianne and Kimberly Boghossian for assistance maintaining and genotyping mice; Dr. Antonello Bonci, Dr. Yeka Aponte, and their lab members for help addressing reviewers' concerns; and Elaine Nguyen for help with tracer injections. We would like to thank Mio Akasako for her key assistance with the retrolabeling experiments. This work was supported by the NIH (GM076430, EY027202, EY012793, and EY017137), the generous contributions of the Alcon Research Institute (to D.M.B.), PEW Charitable Trusts (to D.C.F.), the NSF (I2011104359 to P.M.F.), and the intramural research at the National Institute of Mental Health.

AUTHOR CONTRIBUTIONS

D.C.F. performed behavioral tests, circadian analysis, and immunohistochemical analysis of gene expression. P.M.F. and L.L.O. carried out tracing experiments. D.C.F. and M.B.T. did RNA-seq analysis. L.L.O. and J.Z. performed fiber photometry recording. D.C.F., R.M.L., D.S., J.H.S., and A.K. performed electrophysiological experiments. D.C.F., P.M.F., L.L.O., D.M.B., H.Z., and S.H. wrote the paper.

DECLARATION OF INTERESTS

The authors declare no competing interests.

Received: December 12, 2017
Revised: May 3, 2018
Accepted: August 2, 2018
Published: August 30, 2018

REFERENCES

Altimus, C.M., Güler, A.D., Villa, K.L., McNeill, D.S., Legates, T.A., and Hattar, S. (2008). Rods-cones and melanopsin detect light and dark to modulate sleep independent of image formation. Proc. Natl. Acad. Sci. USA *105*, 19998–20003.

Anders, S., Pyl, P.T., and Huber, W. (2015). HTSeq-A Python framework to work with high-throughput sequencing data. Bioinformatics *31*, 166–169.

Bedrosian, T.A., Fonken, L.K., Walton, J.C., Haim, A., and Nelson, R.J. (2011). Dim light at night provokes depression-like behaviors and reduces CA1

dendritic spine density in female hamsters. Psychoneuroendocrinology *36*, 1062–1069.

Berson, D.M., Dunn, F.A., and Takao, M. (2002). Phototransduction by retinal ganglion cells that set the circadian clock. Science *295*, 1070–1073.

Can, A., Dao, D.T., Terrillion, C.E., Piantadosi, S.C., Bhat, S., and Gould, T.D. (2012). The tail suspension test. J. Vis. Exp. (59), 3769.

Charan, J., and Kantharia, N.D. (2013). How to calculate sample size in animal studies? J. Pharmacol. Pharmacother. *4*, 303–306.

Chawla, S. (2002). Regulation of gene expression by Ca2+ signals in neuronal cells. Eur. J. Pharmacol. *447*, 131–140.

Chen, S.-K., Badea, T.C., and Hattar, S. (2011). Photoentrainment and pupillary light reflex are mediated by distinct populations of ipRGCs. Nature *476*, 92–95.

Choi, S.H., Chung, S., Cho, J.H., Cho, Y.H., Kim, J.W., Kim, J.M., Kim, H.J., Kim, H.J., and Shin, K.H. (2013). Changes in c-Fos expression in the forced swimming test: common and distinct modulation in rat brain by desipramine and citalopram. Korean J. Physiol. Pharmacol. *17*, 321–329.

Coogan, A.N., and Piggins, H.D. (2003). Circadian and photic regulation of phosphorylation of ERK1/2 and Elk-1 in the suprachiasmatic nuclei of the Syrian hamster. J. Neurosci. *23*, 3085–3093.

Davidson, R.J., Pizzagalli, D., Nitschke, J.B., and Putnam, K. (2002). Depression: perspectives from affective neuroscience. Annu. Rev. Psychol. *53*, 545–574.

Dobin, A., Davis, C.A., Schlesinger, F., Drenkow, J., Zaleski, C., Jha, S., Batut, P., Chaisson, M., and Gingeras, T.R. (2013). STAR: Ultrafast universal RNA-seq aligner. Bioinformatics *29*, 15–21.

Ecker, J.L., Dumitrescu, O.N., Wong, K.Y., Alam, N.M., Chen, S.-K., LeGates, T., Renna, J.M., Prusky, G.T., Berson, D.M., and Hattar, S. (2010). Melanopsin-expressing retinal ganglion-cell photoreceptors: cellular diversity and role in pattern vision. Neuron *67*, 49–60.

Faul, F., Erdfelder, E., Buchner, A., and Lang, A.-G. (2009). Statistical power analyses using G*Power 3.1: tests for correlation and regression analyses. Behav. Res. Methods *41*, 1149–1160.

Fernandez, F., Lu, D., Ha, P., Costacurta, P., Chavez, R., Heller, H.C., and Ruby, N.F. (2014). Dysrhythmia in the suprachiasmatic nucleus inhibits memory processing. Science *346*, 854–857.

Fernandez, D.C., Chang, Y.-T., Hattar, S., and Chen, S.-K. (2016). Architecture of retinal projections to the central circadian pacemaker. Proc. Natl. Acad. Sci. USA *113*, 6047–6052.

Francis, T.C., and Lobo, M.K. (2017). Emerging role for nucleus accumbens medium spiny neuron subtypes in depression. Biol. Psychiatry *81*, 645–653.

Franklin, K., and Paxinos, G. (2012). Paxinos and Franklin's the Mouse Brain in Stereotaxic Coordinates, Fourth Edition (Academic Press).

Frodl, T., Scheuerecker, J., Albrecht, J., Kleemann, A.M., Müller-Schunk, S., Koutsouleris, N., Möller, H.-J., Brückmann, H., Wiesmann, M., and Meisenzahl, E. (2009). Neuronal correlates of emotional processing in patients with major depression. World J. Biol. Psychiatry *10*, 202–208.

Güler, A.D., Ecker, J.L., Lall, G.S., Haq, S., Altimus, C.M., Liao, H.-W., Barnard, A.R., Cahill, H., Badea, T.C., Zhao, H., et al. (2008). Melanopsin cells are the principal conduits for rod-cone input to non-image-forming vision. Nature *453*, 102–105.

Hammar, A., and Ardal, G. (2009). Cognitive functioning in major depression–a summary. Front. Hum. Neurosci. *3*, 26.

Hattar, S., Liao, H.W., Takao, M., Berson, D.M., and Yau, K.W. (2002). Melanopsin-containing retinal ganglion cells: architecture, projections, and intrinsic photosensitivity. Science *295*, 1065–1070.

Hattar, S., Lucas, R.J., Mrosovsky, N., Thompson, S., Douglas, R.H., Hankins, M.W., Lem, J., Biel, M., Hofmann, F., Foster, R.G., and Yau, K.W. (2003). Melanopsin and rod-cone photoreceptive systems account for all major accessory visual functions in mice. Nature *424*, 76–81.

Hattar, S., Kumar, M., Park, A., Tong, P., Tung, J., Yau, K.-W., and Berson, D.M. (2006). Central projections of melanopsin-expressing retinal ganglion cells in the mouse. J. Comp. Neurol. *497*, 326–349.

Hillhouse, T.M., and Porter, J.H. (2015). A brief history of the development of antidepressant drugs: from monoamines to glutamate. Exp. Clin. Psychopharmacol. *23*, 1–21.

Huang, Y.-H., Cheng, C.-Y., Hong, C.-J., and Tsai, S.-J. (2004). Expression of c-Fos-like immunoreactivity in the brain of mice with learned helplessness. Neurosci. Lett. *363*, 280–283.

Huang, W., Sherman, B.T., and Lempicki, R.A. (2009). Systematic and integrative analysis of large gene lists using DAVID bioinformatics resources. Nat. Protoc. *4*, 44–57.

Izumo, M., Pejchal, M., Schook, A.C., Lange, R.P., Walisser, J.A., Sato, T.R., Wang, X., Bradfield, C.A., and Takahashi, J.S. (2014). Differential effects of light and feeding on circadian organization of peripheral clocks in a forebrain Bmal1 mutant. eLife *3*. https://doi.org/10.7554/eLife.04617.

Jaeger, J., Berns, S., Uzelac, S., and Davis-Conway, S. (2006). Neurocognitive deficits and disability in major depressive disorder. Psychiatry Res. *145*, 39–48.

Kako, K., and Ishida, N. (1998). The role of transcription factors in circadian gene expression. Neurosci. Res. *31*, 257–264.

Kerestes, R., Harrison, B.J., Dandash, O., Stephanou, K., Whittle, S., Pujol, J., and Davey, C.G. (2014). Specific functional connectivity alterations of the dorsal striatum in young people with depression. Neuroimage Clin. *7*, 266–272.

Kim, D., Song, I., Keum, S., Lee, T., Jeong, M.J., Kim, S.S., McEnery, M.W., and Shin, H.S. (2001). Lack of the burst firing of thalamocortical relay neurons and resistance to absence seizures in mice lacking alpha(1G) T-type Ca(2+) channels. Neuron *31*, 35–45.

Kim, Y., Perova, Z., Mirrione, M.M., Pradhan, K., Henn, F.A., Shea, S., Osten, P., and Li, B. (2016). Whole-brain mapping of neuronal activity in the learned helplessness model of depression. Front. Neural Circuits *10*, 3.

Kurlansik, S.L., and Ibay, A.D. (2012). Seasonal affective disorder. Am. Fam. Physician *86*, 1037–1041.

Lazzerini Ospri, L., Prusky, G., and Hattar, S. (2017). Mood, the circadian system, and melanopsin retinal ganglion cells. Annu. Rev. Neurosci. *40*, 539–556.

LeGates, T.A., Altimus, C.M., Wang, H., Lee, H.-K., Yang, S., Zhao, H., Kirkwood, A., Weber, E.T., and Hattar, S. (2012). Aberrant light directly impairs mood and learning through melanopsin-expressing neurons. Nature *491*, 594–598.

LeGates, T.A., Fernandez, D.C., and Hattar, S. (2014). Light as a central modulator of circadian rhythms, sleep and affect. Nat. Rev. Neurosci. *15*, 443–454.

Love, M.I., Huber, W., and Anders, S. (2014). Moderated estimation of fold change and dispersion for RNA-seq data with DESeq2. Genome Biol. *15*, 550.

Matsuda, S., Peng, H., Yoshimura, H., Wen, T.C., Fukuda, T., and Sakanaka, M. (1996). Persistent c-fos expression in the brains of mice with chronic social stress. Neurosci. Res. *26*, 157–170.

Melrose, S. (2015). Seasonal affective disorder: an overview of assessment and treatment approaches. Depress. Res. Treat. *2015*, 178564.

Meng, C., Brandl, F., Tahmasian, M., Shao, J., Manoliu, A., Scherr, M., Schwerthöffer, D., Bäuml, J., Förstl, H., Zimmer, C., et al. (2014). Aberrant topology of striatum's connectivity is associated with the number of episodes in depression. Brain *137*, 598–609.

Morin, L.P. (2013). Neuroanatomy of the extended circadian rhythm system. Exp. Neurol. *243*, 4–20.

Morin, L.P., and Studholme, K.M. (2014). Retinofugal projections in the mouse. J. Comp. Neurol. *522*, 3733–3753.

Nagalski, A., Puelles, L., Dabrowski, M., Wegierski, T., Kuznicki, J., and Wisniewska, M.B. (2016). Molecular anatomy of the thalamic complex and the underlying transcription factors. Brain Struct. Funct. *221*, 2493–2510.

Noseda, R., Kainz, V., Jakubowski, M., Gooley, J.J., Saper, C.B., Digre, K., and Burstein, R. (2010). A neural mechanism for exacerbation of headache by light. Nat. Neurosci. *13*, 239–245.

Provencio, I., Rodriguez, I.R., Jiang, G., Hayes, W.P., Moreira, E.F., and Rollag, M.D. (2000). A novel human opsin in the inner retina. J. Neurosci. *20*, 600–605.

Quina, L.A., Tempest, L., Ng, L., Harris, J.A., Ferguson, S., Jhou, T.C., and Turner, E.E. (2015). Efferent pathways of the mouse lateral habenula. J. Comp. Neurol. *523*, 32–60.

Roh, S.-C., Park, E.-J., Shim, M., and Lee, S.-H. (2016). EEG beta and low gamma power correlates with inattention in patients with major depressive disorder. J. Affect. Disord. *204*, 124–130.

Roth, B.L. (2016). DREADDs for neuroscientists. Neuron *89*, 683–694.

Ruby, N.F., Hwang, C.E., Wessells, C., Fernandez, F., Zhang, P., Sapolsky, R., and Heller, H.C. (2008). Hippocampal-dependent learning requires a functional circadian system. Proc. Natl. Acad. Sci. USA *105*, 15593–15598.

Russo, S.J., and Nestler, E.J. (2013). The brain reward circuitry in mood disorders. Nat. Rev. Neurosci. *14*, 609–625.

Schmidt, T.M., Chen, S.-K., and Hattar, S. (2011). Intrinsically photosensitive retinal ganglion cells: many subtypes, diverse functions. Trends Neurosci. *34*, 572–580.

Schwarz, L.A., Miyamichi, K., Gao, X.J., Beier, K.T., Weissbourd, B., DeLoach, K.E., Ren, J., Ibanes, S., Malenka, R.C., Kremer, E.J., and Luo, L. (2015). Viral-genetic tracing of the input-output organization of a central noradrenaline circuit. Nature *524*, 88–92.

Scott, A.J., Monk, T.H., and Brink, L.L. (1997). Shiftwork as a risk factor for depression: a pilot study. Int. J. Occup. Environ. Health *3* (*Suppl 2*), S2–S9.

Shen, X., Reus, L.M., Cox, S.R., Adams, M.J., Liewald, D.C., Bastin, M.E., Smith, D.J., Deary, I.J., Whalley, H.C., and McIntosh, A.M. (2017). Subcortical volume and white matter integrity abnormalities in major depressive disorder: findings from UK Biobank imaging data. Sci. Rep. *7*, 5547.

Sherman, S.M. (2001). Tonic and burst firing: dual modes of thalamocortical relay. Trends Neurosci. *24*, 122–126.

Shrestha, P., Mousa, A., and Heintz, N. (2015). Layer 2/3 pyramidal cells in the medial prefrontal cortex moderate stress induced depressive behaviors. eLife *4*. https://doi.org/10.7554/eLife.08752.

Travnickova-Bendova, Z., Cermakian, N., Reppert, S.M., and Sassone-Corsi, P. (2002). Bimodal regulation of mPeriod promoters by CREB-dependent signaling and CLOCK/BMAL1 activity. Proc. Natl. Acad. Sci. USA *99*, 7728–7733.

Vandewalle, G., Schwartz, S., Grandjean, D., Wuillaume, C., Balteau, E., Degueldre, C., Schabus, M., Phillips, C., Luxen, A., Dijk, D.J., and Maquet, P. (2010). Spectral quality of light modulates emotional brain responses in humans. Proc. Natl. Acad. Sci. USA *107*, 19549–19554.

Venzala, E., García-García, A.L., Elizalde, N., Delagrange, P., and Tordera, R.M. (2012). Chronic social defeat stress model: behavioral features, antidepressant action, and interaction with biological risk factors. Psychopharmacology (Berl.) *224*, 313–325.

Vertes, R.P., Linley, S.B., and Hoover, W.B. (2015). Limbic circuitry of the midline thalamus. Neurosci. Biobehav. Rev. *54*, 89–107.

Voorn, P., Vanderschuren, L.J.M.J., Groenewegen, H.J., Robbins, T.W., and Pennartz, C.M.A. (2004). Putting a spin on the dorsal-ventral divide of the striatum. Trends Neurosci. *27*, 468–474.

Wagner, F., Weiss, T., and Veh, R.W. (2017). Electrophysiological properties of neurons and synapses in the lateral habenular complex (LHb). Pharmacol. Biochem. Behav. *162*, 38–45.

Wässle, H. (2004). Parallel processing in the mammalian retina. Nat. Rev. Neurosci. *5*, 747–757.

Wilsbacher, L.D., Yamazaki, S., Herzog, E.D., Song, E.-J., Radcliffe, L.A., Abe, M., Block, G., Spitznagel, E., Menaker, M., and Takahashi, J.S. (2002). Photic and circadian expression of luciferase in mPeriod1-luc transgenic mice invivo. Proc. Natl. Acad. Sci. USA *99*, 489–494.

Xia, Z., Dudek, H., Miranti, C.K., and Greenberg, M.E. (1996). Calcium influx via the NMDA receptor induces immediate early gene transcription by a MAP kinase/ERK-dependent mechanism. J. Neurosci. *16*, 5425–5436.

Zhang, Y., Narayan, S., Geiman, E., Lanuza, G.M., Velasquez, T., Shanks, B., Akay, T., Dyck, J., Pearson, K., Gosgnach, S., et al. (2008). V3 spinal neurons establish a robust and balanced locomotor rhythm during walking. Neuron *60*, 84–96.

STAR★METHODS

KEY RESOURCES TABLE

REAGENT or RESOURCE	SOURCE	IDENTIFIER
Antibodies		
anti-Brn3a	Millipore	Cat #MAB1585; RRID: AB_94166
anti-cFos	Calbiochem	Cat #Ab-5; RRID: AB_2106755
anti-cFos	EnCor	Cat #MCA-2H2; RRID: AB_2571561
anti-GFP	Abcam	Cat #Ab13970; RRID: AB_300798
anti-GRID2IP	Bioss	Cat #bs-11347R
anti-Melanopsin	Advanced Targeting	Cat #AB-N38; RRID: AB_1608077
Anti-NPY	Peninsula Lab	Cat #T-4070; RRID: AB_518504
anti-pCREB-ser133	Cell signaling	Cat #9198; RRID: AB_2561044
anti-pELK-1-Ser383	Cell Signaling	Cat #9181; RRID: AB_2099016
anti-PER1	A generous gift from Dr. David Weaver	N/A
anti-PER2	Alpha Diagnostic	Cat #PER21-A; RRID: AB_1875482
anti-pH3-Ser10	Cell signaling	Cat #D2C8; RRID: AB_10694226
anti-PKC delta	Abcam	Cat #ab182126
anti-RFP	MBL	Cat #PM005; RRID: AB_591279
anti-Vglut2	Millipore	Cat #AB2251; RRID: AB_2665454
Bacterial and Virus Strains		
AAV1/hSyn-HI-eGFP-Cre-WPRE.SV40	Penn Vector Core	Cat #AV-1-PV1848
AAV1/CAG-Flex-GCaMP6f-WPRE.SV40	University of Pennsylvania viral core	Cat #AV-1-PV2816
AAV1/hSyn-HI-eGFP-Cre-WPRE.SV40	Penn Vector Core	N/A
AAV1/Syn-GCaMP6m-WPRE.SV40	University of Pennsylvania viral core	Cat #AV-1-PV2823
AAV2/synP-DIO-sTpEpB.WPRE.bGH	Penn Vector Core	N/A
AAV5/CAG-Flex-GCaMP6f.WPRE.SV40	University of Pennsylvania viral core	Cat #AV-5-PV2816
AAV8.2/EF1a-DIO-synaptophysin-tdTomato	McGovern Institute Viral core	Cat #AAV1
AAVDJ/EF1a-DIO-GCaMP6f	Stanford University viral core	Cat #GVVC-AAV-093
CAV2/cre	Institut de Génétique Moléculaire de Montpellier CNRS UMR	N/A
EnvA G-deleted Rabies-mCherry	Salk Vector Core	N/A
HSV/cre	McGovern Institute Viral core	Cat #RN425
rAAV2/hSyn-hChR2(H134R)-YFP-WPREpA	UNC Vector Core	N/A
rAAV5/hSyn-DIO-hm3D-mCherry	UNC Vector Core	N/A
rAAV5/Syn-Cre-GFP	UNC Vector Core	N/A
Chemicals, Peptides, and Recombinant Proteins		
3,3′-diaminobenzidine	Sigma	Cat #D8001
4OH-tamoxifen	Sigma	Cat #H7904
AntiFade medium	Molecular Probes	Cat #P36980
Avertin (2, 2, 2-Tribromoethanol	Sigma	Cat #T48402
Biocytin	Sigma	Cat #B4261
Cholera toxin β-subunit (CTβ) fluorescently conjugated	ThermoFisher	Cat #C22842; C22841
Clozapine-N-oxide	Sigma	Cat #C0832
Normal Goat Serum	Vector Labs	Cat #S-1000

(*Continued on next page*)

Continued

REAGENT or RESOURCE	SOURCE	IDENTIFIER
Paraformaldehyde	Electron Microscopy Sciences	N/A
Tamoxifen	Sigma	Cat #T5648
Critical Commercial Assays		
Ribo-Zero Gold rRNA Removal Kit	Illumina	Cat #MRZG126
RNeasy Lipid Tissue Mini Kit	QIAGEN	Cat #74804
TruSeq RNA Library Prep Kit v2	Illumina	Cat #RS-122-2001
Vectastain HRP kit	Vector Labs	Cat #PK-6101
Deposited Data		
Raw and analyzed (SCN) RNA-seq data	This paper GSE113875	N/A
Mus musculus reference genome (mm10)	UCSC Genome Browser https://genome.ucsc.edu/cgi-bin/hgGateway?db=mm10	N/A
Experimental Models: Organisms/Strains		
Mouse: C57BL/6J	The Jackson laboratory	Cat #000664
Mouse: CD-1	Charles River labs	Cat #022
Mouse: *cFos*^{CreERT2}	The Jackson laboratory	Cat #021882
Mouse: *Opn4*$^{aDTA/aDTA}$	Generated in the laboratory of Dr. Hattar	N/A
Mouse: *Opn4*$^{Cre/+}$;*Brn3b*$^{zDTA/+}$	Generated in the laboratory of Dr. Hattar	N/A
Mouse: *Opn4*^{CreERT2}	Generated in the laboratory of Dr. Hattar	N/A
Mouse: *ROSA*$^{Synaptophysin\text{-}tdTomato}$	The Jackson laboratory	Cat #012570
Software and Algorithms		
Adobe Photoshop	Adobe Systems	N/A
ANY-maze Behavioral tracking software	Stoelting Co.	N/A
ClockLab	Actimetrics, IL	N/A
Database for Annotation, Visualization and Integrated Discovery (DAVID)	Huang et al., 2009 https://david.ncifcrf.gov	N/A
DESeq2	Love et al., 2014 https://bioconductor.org/packages/release/bioc/html/DESeq2.html	N/A
G*Power	Faul et al., 2009 Version 3.1	N/A
GRAPHIC STATE Software for Behavioral Research	Coulbourn Version 2.101	N/A
GraphPad Prism 7.04	GraphPad software	N/A
HTSeq-count	Anders et al., 2015 https://github.com/simon-anders/htseq	N/A
IgorPro	Wavemetrics	N/A
ImageJ software	NIH, USA	N/A
MAtlab	Mathworks	N/A
Origin	OriginLab	N/A
STAR v2.4	Dobin et al., 2013 https://github.com/alexdobin/STAR	N/A
VitalView software	Mini Mitter, OR	N/A
Zeiss Zen software	Zeiss	N/A
Other		
23-Watt compact fluorescent light bulbs	GE Daylight	Cat #FLE10HT3/2/D
Coronal slice brain matrix	Kent Scientific	Cat #RBMA-200C
Coulbourn precision animal shocker	Coulbourn	Cat #H13-17A
Hamilton syringe	Hamilton	Cat #701 LT SYR
Light meter	EXTECH	Cat #401025
Microcapillary tube	Sigma	Cat #P0674

CONTACT FOR REAGENT AND RESOURCE SHARING

Further information and requests for resources and reagents should be directed to and will be fulfilled by the Lead Contact, Samer Hattar (samer.hattar@nih.gov).

EXPERIMENTAL DESIGN AND SUBJECT DETAILS

Animals

Mice were housed under a 12 h light:12 h dark (T24) cycle at a temperature of 22°C with food and water *ad libitum*. Wild-type mice of a mixed background (B6/129 F1 hybrid; Jackson Laboratory) were used in this study. *Opn4*$^{Cre/+}$;*Brn3b*$^{zDTA/+}$ mouse line was previously described (Chen et al., 2011). Briefly, we have shown that ~200 M1 ipRGCs, which are the only ipRGCs that do not express the transcription factor *Brn3b* (POU4F2) (Schmidt et al., 2011), exclusively innervate the SCN (Chen et al., 2011). Mice that express the *Cre*-dependent diphtheria toxin (DTA) under the control of the *Brn3b* promoter (*Brn3b*$^{zDTA/+}$), were mated with *Opn4*$^{Cre/Cre}$ mice to obtain *Opn4*$^{Cre/+}$;*Brn3b*$^{zDTA/+}$ mice, where *Brn3b*-negative cells are the only ipRGCs to survive. *Opn4*$^{aDTA/aDTA}$ mouse line was previously described (Güler et al., 2008). *ROSA*$^{Synaptophysin\text{-}tdTomato}$ mice (Jackson laboratory, Stock No: 012570) were mated with *Opn4*^{CreERT2} mice (Ecker et al., 2010) to generate a mouse line (*Opn4*$^{CreERT2/+}$;*ROSA*$^{Synaptophysin\text{-}tdTomato}$) in which most ipRGCs expresses the fused protein (induced by high doses of Tam) in axonal terminals. Mice that express tetX in a *Cre*-dependent manner (*R26*^{tetX}) were previously described (Zhang et al., 2008). All animals were handled in accordance with guidelines of the Animal Care and Use Committees of Johns Hopkins University, University of Maryland, Brown University, and the National Institute of Mental Health (NIMH). All efforts were made to minimize the pain and the number of animals used. Calculation of sample size per experiment was determined, or confirm by post hoc analyses, using a G*Power 3 software (Charan and Kantharia, 2013; Faul et al., 2009).

Rhythmic activity measurement

Single-housed mice were exposed to the T24 and/or T7 cycles, and light intensity was kept ~500 lux (provided by Philips Daylight deluxe fluorescent lamps), measured using a light meter (EXTECH Foot Candle/Lux Light Meter, 401025). The general activity of mice was monitored using infrared motion detectors from Mini Mitter (Respironics) mounted to the top of the cages. Data was collected in 10-min bins using VitalView software (Mini Mitter, OR). The total activity and period lengths were calculated using ClockLab (Actimetrics, IL).

Chronic control of PHb function

Silencing of PHb neurons

Mice that express tetX/GFP in a *Cre*-dependent manner, and littermate controls, were stereotaxically injected with an AAV5/Cre in the PHb region (bilateral injections). Four weeks post injection, mice were exposed to T24 or the T7 cycles.

Chronic DREADD strategy

c-Fos^{CreERT2} and littermate *Cre*-negative (Control) mice were stereotaxically injected with a Cre-dependent AAV5/DIO-hM3D-mCherry in the PHb region (bilateral injections). A week later, mice were subjected to a light pulse (15-min, 1000 lux, CT14), and immediately injected with 4OH-tamoxifen (50 mg/kg i.p., H7904 Sigma) to induce *Cre*-recombination. After the light pulse, mice were in darkness for 24 hours, and then kept under T24 cycle for 4 weeks, before starting with the experiments. *c-Fos*^{CreERT2} mice injected with the AAV that received 4OH-Tam, but without the light pulse exposure, were used as control of non-light-mediated c-Fos induction.

CNO in drinking water

The effectiveness of clozapine-N-oxide (CNO, C0832 Sigma) dissolved in drinking water (5 μg/ml) was compared to CNO i.p. injections. For that, c-Fos induction (in AAV-infected neurons) was immunohistochemically evaluated in mice that were perfused either 12 hours after been exposed (and having access) to CNO dissolved in drinking water, or 2 hours after a single i.p. injection of CNO (1mg/kg); in both cases, mice were kept in constant darkness during the experiment. To achieve chronic DREADD control, water + CNO was given to mice during 14 days, and fresh solution was daily replaced (10 mL per day). The consumption of water + CNO was daily measured.

CNO i.p. injections

In a different set of experiments, 4 weeks after light pulse + 4OH-Tam administration, CNO was intraperitoneally (i.p.) injected (1mg/kg) twice a day (CT 13, and CT 18), during 14 days. To minimize the stress effect, tuberculin syringes were used.

Behavioral test

Single-housed mice were kept under the T24 or T7 cycles for 2 weeks before testing, as previously described (LeGates et al., 2012). The general activity of mice was monitored using infrared sensors and behavioral tests were performed between CT 12 - 14 (during active phase). In all cases, room was illuminated using dim red lamps.

Mood-related behavior

Opn4$^{Cre/+}$ and *Opn4*$^{Cre/+}$;*Brn3b*$^{zDTA/+}$ mice were tested for either the sucrose preference, TST or the FST. TetX mice (and respective controls) were first evaluated for sucrose preference followed by either TST or FST. Mice with chronic activation of PHb neurons (AAV DREADD and their respective controls) that received CNO in drinking water were exposed to either the TST or FST.

Sucrose Preference

Mice were acclimated to the 2-bottle water delivery system for 3 days. Sucrose preference was then assessed over two consecutive days. Each day, one bottle containing 1% sucrose and one bottle containing water was introduced at the beginning of the active phase of mice. Sucrose preference was calculated by dividing the amount of sucrose consumed by the total volume consumed (water + sucrose).

Tail suspension

Mice were suspended by the tail using tape. White chambers prevented interaction between them. A maximum of six animals were tested simultaneously. Mouse activity was recorded during 6 min. At the end of the session, mice were placed back in their home cages. Immobility time was analyzed manually following the criteria described in Can et al. (2012).

Forced swim test

Mice were placed in an inescapable container of water (25°C) for 6 min. Behavioral response was monitored using a video camera positioned in front of the apparatus and scored using a computerized video tracking system (ANYmaze). Time spent immobile for the last 4 min of the test was calculated.

Cognitive function tests

mice were tested for both the NOR test and the MWM. All behavioral tests were performed in a blind manner by a single observer.

Novel Object recognition test

On day 1, mice were placed in an open arena (40 cm x 30 cm) and were allowed to explore during 10 minutes before being returned to their home cage. On day 2, mice were placed in the same open arena with two identical objects. After 10 minutes, mice were returned to their home cage. After an hour, mice were placed back in the arena for 5 minutes with the familiar object and a novel object. Mice were monitored and tracked for object exploration and the time was calculated for the percentage of time spent with the novel versus the familiar object (ANYmaze software). At the end of the experiment, mice were placed back in their home cages and the arena and objects were sanitized with 70% v/v ethanol. The objects used in this test had been previously validated using an independent cohort of wild-type mice, which did not display significant preference for any of them.

Morris Water Maze

Mice were placed in a circular pool (150 cm diameter) to swim to a hidden platform (submerged in the pool such that 1cm of water covered the platform hiding it from sight). Four different (in shape and color) cues were attached to the side of the pool equidistant from one another, and the pool was surrounded by a plain curtain to block any other visual cues. Water was mixed with non-toxic white paint to render it opaque. Water temperature was maintained between 20-25°C during experiments by water heaters designed for fish aquariums. On day 0, mice were trained to escape the pool using a visual cue located on top of the platform to familiarize them with the test. Once the mouse either finds the island or swims for 90 s without finding the island, it was removed from the pool and placed back in its cage. This was performed four times with an inter-trial interval of 30 min, and the platform was moved between each trial. During the *acquisition phase*, mice were trained (one trial per day for 12 days) to find the hidden platform using the four visual distal cues surrounding the pool. The mouse was randomly placed in a different area of the pool at the start of each trial with the platform maintained in the same quadrant (target quadrant). Mice were allowed to swim for a maximum of 90 s and supervised for the full time in the pool. The platform was removed on day 13 in the *probe trial*. The swimming in each quadrant (T: target, A1: adjacent 1, A2: adjacent 2, O: opposite, quadrants) and specifically the preference for the target quadrant was measured to evaluate spatial memory using a computerized video tracking system (ANYmaze). *Reversal training* began on day 14 when the platform was moved to the quadrant opposite the original target quadrant. Mice were trained as described for the acquisition phase. During *acquisition phase* and *reversal training,* the latency to find the platform was measured; *probe trial* was analyzed by calculating the percentage time spent in the target quadrant.

Light-independent paradigms of mood alterations

WT mice (3 months old) individually housed in T24 light cycle were exposed to a learned helplessness, forced-swim, or social defeat paradigms at CT 14 (two hours after the beginning of active phase). During the sessions mice were kept in darkness to avoid any light-mediated effect on c-Fos induction. Control mice were perfused at similar CTs.

Learned helplessness paradigm

Mice were exposed to sessions of inescapable foot shocks on two consecutive days, as previously described (Huang et al., 2004; Kim et al., 2016), with minor modifications. Each session consisted of a total of 300 randomized electric foot shocks (300 μA intensity, 1-3 s duration, 5-15 s inter-shock intervals; Coulbourn precision animal shocker) applied during a period of ~60 min. After the second session, mice were kept in darkness for 30 min, and perfused for histochemical analysis.

Forced-swim paradigm

Mice were exposed to two sessions of inescapable swimming on two consecutive days, following Choi et al. (2013), with minor modifications. On day 1, mice were individually placed in a container of water (25°C) for 15 min; after that, mice were returned to their home cages. On day 2, mice were placed in the same pool for 5 min, then kept in darkness for 80 min, and finally perfused.

Social defeat paradigm

Cages with a plastic mesh dividing the arena into two similar areas were used. The protocol used was following Matsuda et al. (1996) and Venzala et al. (2012), with minor modifications. On day 1, an *intruder* C57B6/J mouse was placed into the compartment housing a resident CD1 mouse, allowing physical interaction for 5 minutes. After that, *intruder* mouse was placed on the next compartment of the same cage, allowing sensory contact for 24 hours. This procedure was repeated during 4 consecutive days. On day 4, *intruder* mice were exposed to physical interaction, returned to their home cages and perfused 80 min later.

METHOD DETAILS

Light-mediated gene induction/ protein phosphorylation

T24 and T7 cycles-housed mice (for 2 weeks) were kept in darkness for 1 day to avoid any prior light exposure effect. Two hours after the onset of activity (CT 14), mice were subjected to a 15-min light pulse (1000 lux), using 23-Watt compact fluorescent light bulbs (GE Daylight FLE10HT3/2/D) with a color temperature of 6500 K to simulate natural sunlight. For CREB, ELK-1 and H3 phosphorylation analysis, mice were intracardially perfused with 4% paraformaldehyde immediately after the end of the light pulse, while for PER1 and c-Fos induction, mice were kept in darkness for 90 min after light pulse and then perfused. Coronal brain sections were blocked for 2 hours in 1x PBS containing 3% heat-inactivated goat serum and 0.3% Triton X-100, and then incubated using the following primary antibodies (for 1 day at 4°C): rabbit antibody α-cFos (Calbiochem Ab-5; 1:20000); rabbit antibody α-PER1 (a generous gift from Dr. David Weaver); rabbit α-pCREB-Ser133 (Cell signaling 9198, 1:500); rabbit α-pELK-1-Ser383 (Cell Signaling 9181; 1:1000); rabbit α-pH3-Ser10 (Cell signaling D2C8; 1:1000). The immunohistochemical detection was performed using a Vectastain HRP kit (Vector Labs) based on biotin-streptavidin-peroxidase, and visualized using 3,3′-diaminobenzidine (DAB) as chromogen. Finally, sections were mounted on microscope slides, dehydrated, and coverslipped. For characterization of PHb identity (thalamus versus epithalamus), immunofluorescence analyses were performed as described below. The quantification analyses were performed as described in sections Optical density analysis and c-Fos induction.

PER1/2 rhythmic expression

After T24 or T7 cycles exposure, mice were kept in constant darkness for at least 24 hours to avoid any light mediated gene-induction effects. The general activity of mice was monitored, and animals were perfused at CT 1, 7, 13, or 19. Coronal brain sections were used to assess the levels of clock gene expression in the SCN and PHb. A rabbit antibody α-PER1 or a rabbit α-PER2 (Alpha Diagnostic PER21-A, 1:4000) antibody were used, and the immunohistochemical detection was performed as described above. The analysis was performed as described in the section Optical density analysis.

Immunofluorescence

Brain sections and retinas were incubated in 0.1M PBS with 3% Goat serum (Vector Labs) and 0.3% Triton X-100 (Sigma-Aldrich) for 2 hours, and then incubated using the following antibodies (1-2 days, at 4°C): rabbit α-Melanopsin (Advanced Targeting AB-N38, 1:500); rabbit α-RFP (MBL PM005, 1:1000); chicken α-GFP (AbCam Ab13970, 1:2000); guinea pig IgG α-VGlut2 (Millipore AB2251, 1:1000); mouse IgG1 α-c-Fos (EnCor MCA-2H2, 1:1000); rabbit α-c-Fos (Calbiochem AB-5, 1:1000); mouse IgG1 α-Brn3a (brain-specific homeobox/POU domain protein 3A, Millipore MAB1585, 1:250); rabbit α-GRID2IP (glutamate receptor ionotropic delta 2-interacting protein 1, Bioss bs-11347R, 1:1000); rabbit α-PKCd (AbCam, 1:2000). GRID2IP immunostaining required an antigen retrieval step (citrate buffer, at 85°C for 30 min). After several washing steps, Alexa-conjugated secondary antibodies were used (Molecular Probes, 1:500, for 2 hours at room temperature). Finally, slides were mounted using AntiFade medium (Molecular Probes). Images were acquired using an LSM-510 confocal microscope (Zeiss).

Melanopsin immunohistochemistry and dendritic reconstruction

Retrolabeled RGCs were imaged on a Zeiss LSM 510 confocal microscope. Images were taken at 40x magnification across the depth of the inner plexiform layer (IPL) for each cell (Z stack) to capture dendritic stratification revealed by melanopsin expression. Stacks were imported into Photoshop (Adobe) and reconstructed by tracing immunolabeled dendrites from retrolabeled somas through adjacent planes of the Z stack. Cells with dendrites that branched in only the inner ON sublamina of the IPL were classified as M1 ipRGCs; those with dendrites in both the ON and OFF IPL sublaminae were classified as M3 ipRGCs.

SCN dissection and RNA-sequencing

Mice housed under T24 or T7 cycles were kept in darkness for 1 day, and a light pulse was applied (15 min) at CT14. An hour later, brains were isolated under red dim light and placed ventral side up on an ice-cold coronal slice brain matrix (Kent Scientific). A 1 mm coronal slice of the brain was made with ice-cold razor blades positioned surrounding the optic chiasm. The slice was laid flat on one of the blades and the SCN was collected using a 1mm diameter sample corer (FST) and immediately placed in Qiazol chilled on ice and stored at −80C. SCN tissue samples from 3 mice were pooled for each biological replicate in all conditions. Following dissection, RNA was extracted using a QIAGEN RNeasy lipid tissue mini kit and processed with an Illumina RiboZero Gold kit. Sequencing libraries were prepared with the Illumina TrueSeq RNA-v2 kit. Libraries were multiplexed and sequenced on a Hiseq4000 using 75bp paired-end reads to a depth of at least 130 million reads per sample. Reads were mapped to the mouse reference genome (mm10) with STAR (v2.4.2a) and read counts were generated with htseq-count from the HTSeq python package (v0.9.1). Differential

expression analysis was performed with DESeq2. Gene ontology (GO) analysis was performed using the Database for Annotation, Visualization and Integrated Discovery (DAVID) (Huang et al., 2009).

Retinal injections

Retinal projections were visualized using intravitreal injections (1 μl) of the tracer cholera toxin β-subunit (CTβ) fluorescently conjugated (Alexa Fluor 488 or 594, Thermofisher). AAVs (1 μl) were also injected in order to infect RGCs. Mice were anesthetized by i.p. injections of avertin (2, 2, 2-Tribromoethanol) and placed under a stereo microscope. A glass needle (pulled 10 μL microcapillary tube, Sigma P0674) and a 10 μL Hamilton syringe were used to drive the solution into the vitreous chamber of the eye to ensure delivery specifically to the retina. Mice recovered from injections on a heating pad until they woke from anesthesia. After injections, animals were given 3 to 4 days recovery period. Mice were deeply anesthetized by intraperitoneal (i.p.) injection of avertin (2, 2, 2-Tribromoethanol), and perfused intracardially with 4% paraformaldehyde. Brains were post-fixed overnight in the same fixative, and brain sections were obtained using a cryostat. In some cases, eyes were also removed and retinas were dissected in oxygenated Ames medium (Sigma-Aldrich). Relieving cuts were made to mount retinas flat on a piece of lens paper. Retinas were then incubated in 4% paraformaldehyde (Electron Microscopy Sciences) overnight at 4°C.

Stereotaxic injections

Mice were deeply anesthetized, and CTβ, AAVs or gΔRabies were stereotaxically delivered. All coordinates used follows the Paxinos and Franklin mouse atlas (Franklin and Paxinos, 2012). A 10 μL microcapillary pipette was pulled and loaded with the solution; Injections were performed using a microinjector (Nanojector II, Drummond Scientific Company). A heating pad was used to maintain the body temperature. Before and after surgery, systemic analgesics (buprenorphine, 0.1 mg/kg) were administrated. For anatomical analysis mice were perfused at different times post injection (3-4 days after CTβ injection, 4 weeks after AAVs injection, or 5 days after gΔRabies injection) and the brains were subsequently sectioned on a cryostat. In specific experiments, retinas were also dissected out after perfusion and post-fixed for 1 hour.

Electrophysiology

Mice were intravitreally injected with an AAV2/hSyn-hChR2(H134R)-EYFP (University of North Carolina Vector Core). Three to four weeks post injection, mice were anesthetized and decapitated. Brains were removed into an iced cutting solution, oxigenated with 95% O_2/5% CO_2 containing: (in mM): 234 sucrose, 26 $NaHCO_3$, 11 dextrose, 10 $MgCl_2$, 2.5 KCl, 1.25 NaH_2PO_4, and 0.5 $CaCl_2$. Coronal slices (300 μm) were prepared using a VT1200S vibratome (Leica Microsystems Inc., Buffalo Grove, IL); slices were then incubated for 20 minutes at 34°C immersed in oxygenated artificial cerebrospinal fluid (ACSF) solution containing (in mM): 126 NaCl, 26 $NaHCO_3$, 10 dextrose, 2.5 KCl, 1.5 $MgCl_2$, 1.25 NaH_2PO_4, and 1.15 $CaCl_2$. Slices were then held at room temperature in the same ASCF, and recordings commenced at least thirty minutes after high-temperature incubation. For recordings, slices were perfused with ACSF at ~34°C. Labeled retinal fibers were visualized using oblique deep-red illumination under a 60X water-immersion lens (Olympus) mounted on an Axioskop 2 FS plus upright microscope (Carl Zeiss Microscopy, LLC, Thornwood, NY) equipped with Plan N 4x and LUMFLN 60XW objectives (Olympus, Tokyo, Japan), part 91015 filter cube with set number 49002 EGFP bandpass filter set (Chroma Technology Corporation, Bellows Falls, VT), M470L3 mounted LED controlled by a LEDD1B driver (Thorlabs, Inc., Newton, NJ), and Ximea MQ013MG-E2 digital camera (XIMEA, Münster, Germany). Recording pipettes contained (in mM): 95 $CsCH_3SO_3$ (voltage-clamp recordings) or 95 K D-gluconate (current-clamp recordings), 20 TEA-Cl or 20 mM NaCl (voltage-or current-clamp recordings, respectively), 10 HEPES, 8 PO_4-creatine, 4 Mg-ATP, 1 4-AP, 1 BAPTA, and 0.4 GTP Tris, pH 7.2; 2 QX314 was sometimes added to block voltage-gated Na^+ channels. Neurons were filled with biocytin (0.1%) during the recording session for post hoc morphological reconstruction. Membrane potentials and currents were recorded using a MultiClamp 700B amplifier (Molecular Devices, Sunnyvale, CA). Amplifier output was filtered at 4 kHz and digitized at 20 kHz using an ITC-18 data acquisition interface controlled by custom-written software (Igor Pro; Wavemetrics). Offline analysis was performed using Igor Pro. Holding potentials were corrected for a −10 mV junction potential. Access resistances were typically ~20 MΩ, and were compensated by ~15%–30%. For ChR2 stimulation, the M470L3 mounted LED and LEDD1B driver were triggered using a TTL wave consisting of 2 ms pulses at varying frequencies generated in IGOR Pro. PHb neurons considered to receive retinal input were defined according to their location in an area innervated by retinal fibers (YFP expression), and due to the time-locked nature of the evoked EPSC relative to laser onset (averaged of several trials).

Hippocampal recordings

Opn4$^{Cre/+}$ and *Opn4*$^{Cre/+}$;*Brn3b*$^{zDTA/+}$ mice were exposed to the T24 or T7 cycles for 2 weeks. Mice activity was monitored and samples were obtained at the beginning of the active phase of mice (CT 12-14). Coronal hippocampal slices (0.4 mm) were used to evaluate hippocampal LTP, as previously described (LeGates et al., 2012). Slices were obtained and collected in ice-cold dissection buffer (2.6mM KCl, 1.23mM NaH_2PO_4, 26mM $NaHCO_3$, 212.7mM sucrose, 10mM dextrose, 3mM $MgCl_2$ and 1mM $CaCl_2$, bubbled with 5% CO_2, 95% O_2). For recording, the same buffer was used, except that sucrose was replaced by NaCl, and the temperature raised to 30°C. LTP protocol was delivered after 20 min of stable baseline transmission. Schaffer collaterals were stimulated to obtained synaptic responses in CA1 stratum radiatum (0.33 Hz stimulation, 0.2-ms pulses (concentric bipolar electrodes, FHC)). One or four theta epochs (each epoch consisted of 10 trains of four pulses (at 100 Hz) delivered at 5 Hz) were used to obtain LTP responses.

Fiber Photometry

The fiber photometry apparatus consists of two LEDs (Doric Lenses) emitting 405 and 465 nm light respectively delivering light through a rotary joint to a 200 um optical fiber (Doric Lenses or ThorLabs) implanted in the region of interest in the brain of a freely moving animal; light collected by the fiber passes through a filter/beam splitter (Doric Lenses) capable of separating light in the 420-450 nm range from light in the 500-550 nm range, and is detected by two H10722 photomultiplier tubes (Hamamatsu), one for each frequency range. The signal is digitized and acquired by a computer. Data analysis was carried out with MATLAB (Mathworks) and Origin (OriginLab). Briefly, both the GCaMP6 emission signal and the auto-fluorescence from the tissue were recorded at the same time at a sampling rate of 0.3 kHz. Both were processed with a FFT filter to reduce noise. Auto-fluorescence intensity was transformed by constants determined for each experiment by linear regression of the GCaMP6 signal; it was then subtracted from the GCaMP6 signal in order to remove artifacts. For all the experiments, the same mice were tested for both the T24 and T7 cycles. This avoids any potential variations due to differential transfection and expression levels. In all cases the excitation light was the same between T24 and T7 cycles, and different animal signals were normalized to baseline for averaging.

Optic fiber implantation

After isoflurane anesthesia, the mouse's head was fixed to a stereotaxic apparatus; the skull was exposed after application of povidone/iodine and 70% ethanol; one anchor screw was driven into the skull; a hole was drilled over the region of interest (with coordinates calculated from bregma), and after thorough removal of bone debris, the optical fiber (Doric Lenses, inner diameter = 200 μm, NA = 0.37; or Optogenix, inner diameter = 200 μm, NA = 0.66) was lowered into the brain at a speed of ~200 μm/min. On reaching the appropriate dorsoventral coordinate, the fiber was secured in place by application of dental cement around its exposed portion, encased in a metal ferrule.

QUANTIFICATION AND STATISTICAL ANALYSIS

Morphometric analysis

For all morphometric image processing, digitalized captured TIF-images were assembled and processed with Zeiss Zen software (Zeiss) and/or Adobe Photoshop (Adobe Systems), and transferred to ImageJ software (NIH, USA). Sample analysis was performed with the experimenter blind to condition. All the nomenclature used in the manuscript follows that of Franklin and Paxinos (2012).

Optical density analysis

Digital images were obtained using an inverted microscope (Zeiss Axioimager.M1), converted to 8-bits gray scale and the optic density (relative to total area) was measured. For both the SCN and PHb, total area of analysis was manually outlined in coronal brain sections. In all cases, 3 independent sections per animal were quantified and averaged.

Light-mediated c-Fos induction

For both the SCN and PHb, total area of analysis was manually outlined in coronal brain sections. For the SCN, bilateral nuclei were evaluated; and for the PHb only one side of the coronal section was evaluated. Results obtained from 3 separate sections/nucleus were averaged per animal.

Characterization of light-induced c-Fos expression in PHb neurons

Total area of analysis was manually outlined in coronal brain sections. Double positive PHb cells (c-Fos(+), Brn3a(+) or c-Fos(+), GRID2(+)) were quantified relative to total number of c-Fos(+) cells. Results obtained from 5 separate sections/animal were averaged.

c-Fos induction in light-independent models of depression

The number of c-Fos(+) cells were evaluated in the PHb, LHb, and vmPFC. As described above, three different protocols known to induce mood alterations were used. For the PHb, total area of analysis was manually outlined; the total LHb area was used for quantification; whereas an area of 1.21 × 0.64 mm was used for the vmPFC. In all cases, the number of c-Fos(+) cells was obtained from only one side of these bilateral structures. Results obtained from 5-6 separate sections/nucleus were averaged per animal.

Statistical Analysis

Statistical analysis of results was made by using unpaired Student's t test, analysis of variance (ANOVA), followed by Tukey's or Dunnett's tests, as stated. For the Sucrose preference and NOR tests, a One sample t test compared to a 'test value' = 50 was also performed. All the analyses were done using GraphPad Prism, version 7

RNA-seq differential expression testing was performed in DESeq2 with a Wald test followed by p value adjustment for false discovery rate using the Benjamini-Hochberg procedure, as described (Love et al., 2014).

DATA AND SOFTWARE AVAILABILITY

The accession number for the raw and processed gene expression data from the RNA-sequencing experiments reported in this paper is GEO: GSE113875. Data from this study are available from the corresponding author upon request.

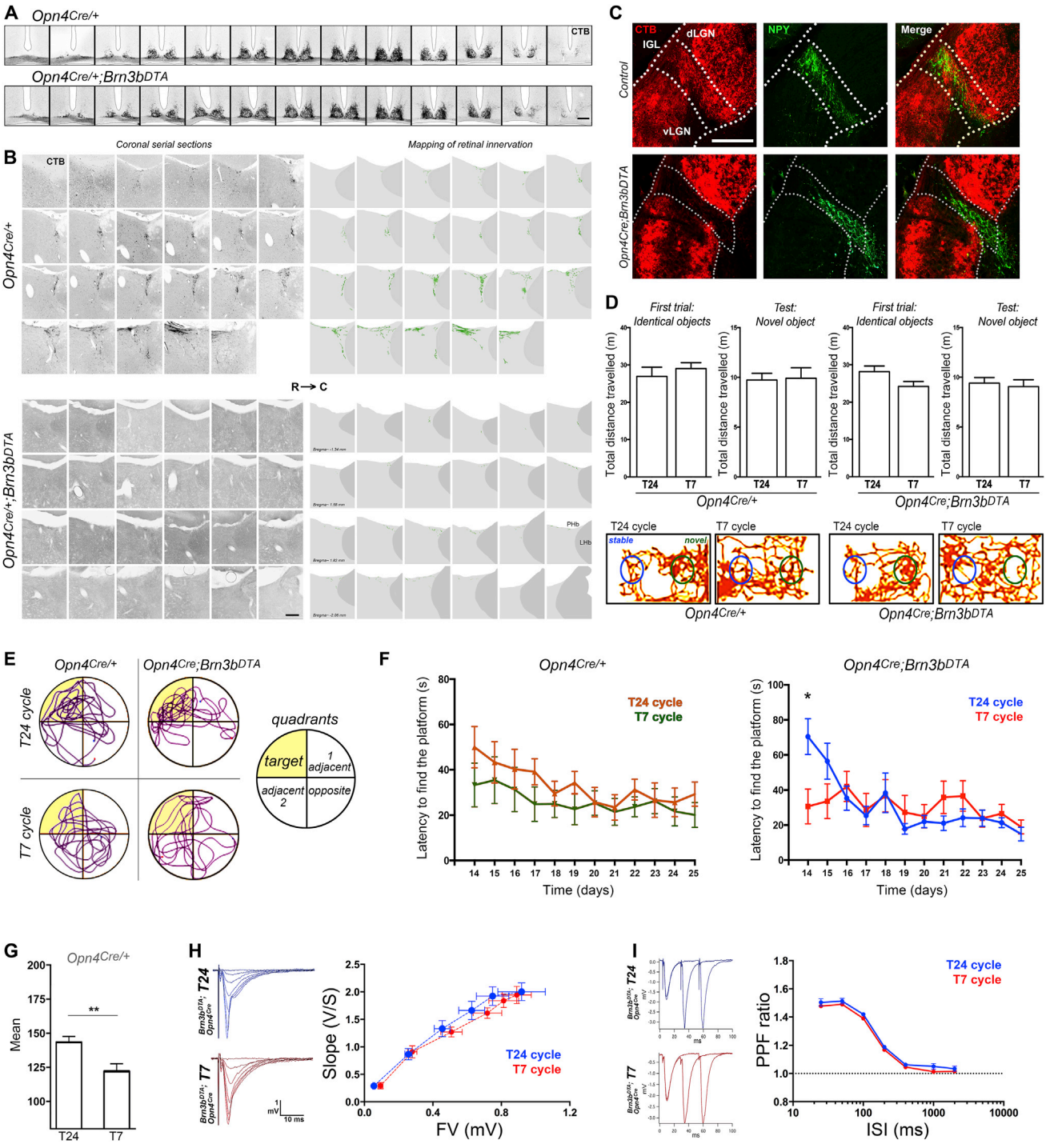


Figure S1. T7 Cycle-Housed *Opn4*^{Cre};*Brn3b*^{zDTA} Mice Showed Hippocampal Learning and Functional Deficits, Related to Figure 1

(A-C) CTβ was intravitreally injected in *Opn4*$^{Cre/+}$ and *Opn4*$^{Cre/+}$;*Brn3b*$^{zDTA/+}$ mice in order to trace retinal fibers. A complete serial sectioning of the SCN (A) and PHb region (B), and a reconstruction of retinal innervation (B, green), are shown. A dense retinal innervation was observed throughout the SCN in both groups of mice (A), whereas a drastic reduction in retinal innervation in the PHb was observed in *Opn4*$^{Cre/+}$;*Brn3b*$^{zDTA/+}$ mice. C: Neuropeptide Y (NPY) staining was used for delineating the intergeniculate leaflet (IGL). As shown in the representative images, a substantial reduction in the retinal innervation to the IGL, compared with the dorsal and ventral LGN, was found in *Opn4*$^{Cre/+}$;*Brn3b*$^{zDTA/+}$ mice. Four adult male mice per group were used to characterize the pattern of retinal projections. (D) For the NOR, the total distance traveled during the first session (familiarization session, mice have 10 min to freely explore two similar objects) and the test session (5 min exploratory time, where one of the objects was replaced by a novel object) were similar for both groups of mice exposed to T24 or T7 cycles. Data

(legend continued on next page)

are mean ± SEM, by Tukey's test. Representative traces of the exploratory activity of mice during the test trial for all groups are shown in the lower panel. Blue line represents the area of the familiar (stable) object, whereas the green line indicates the area with the novel object.

(E) For the MWM, representative traces obtained during the test trial are shown. Target area is represented in yellow.

(F) Results obtained during the reversal phase of the MWM. A comparison between learning (day 12) and reversal (day 14) results was also performed for all groups (*Opn4*$^{Cre/+}$: T24 $p < 0.01$, T7 $p = 0.12$; *Opn4*$^{Cre/+}$;*Brn3b*$^{zDTA/+}$: T24 $p < 0.001$, T7: $p = 0.81$). Data are mean ± SEM. *$p< 0.05$, by Tukey's test.

(G) LTP responses in the hippocampus obtained from *Opn4*$^{Cre/+}$ mice housed under the T24 or T7 cycles (n = 8-12 mice). Data are mean ± SEM. **$p< 0.01$, by Tukey's test.

(H-I) *Opn4*$^{Cre/+}$;*Brn3b*$^{zDTA/+}$ mice housed under the T24 or T7 cycles showed no significant differences in the field potential slope, fiber volley amplitude, input–output function (field potential slope normalized to fiber volley (FV) amplitude) (H), or pair pulse facilitation (PPF) responses (I). ISI, inter-stimulus intervals. Data are mean ± SEM. *$p<0.05$, **$p<0.01$, by Student's t test.

Scale bars: (A) 100 μm; (B, C) 200 μm.

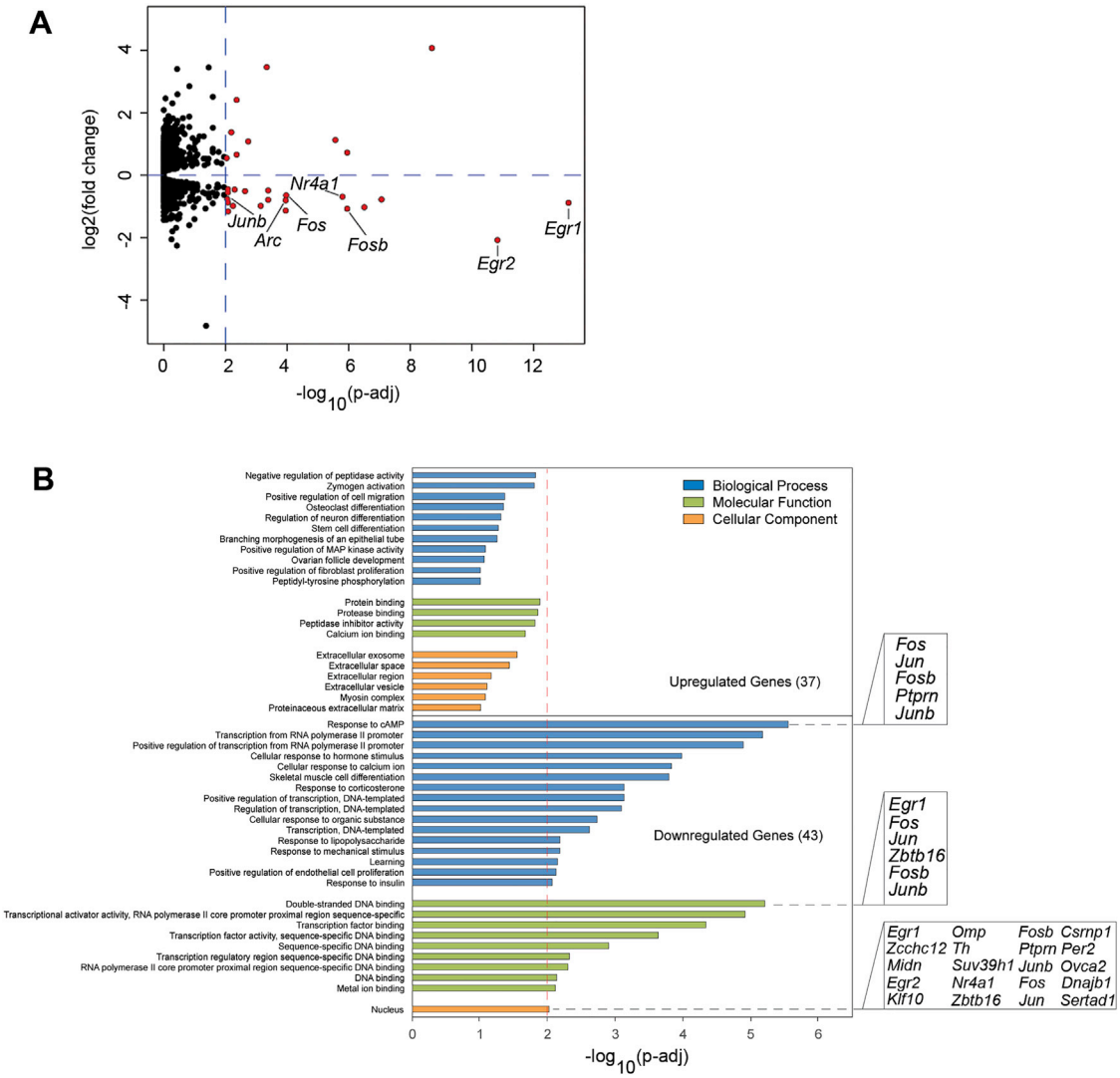


Figure S2. Gene Expression Profile of the SCN, Related to Figure 2

(A) Volcano plot illustrating gene expression differences between SCN samples obtained from T24 versus T7 cycles. All genes with FDR-adjusted $p < 0.01$ are colored in red (9 upregulated genes, 20 downregulated genes). 7 classical immediate early genes are highlighted.

(B) Gene ontology (GO) analysis of differentially expressed genes (80 genes, FDR-adjusted $p < 0.1$) in T7 cycle-housed SCN samples compared to T24-housed samples. Genes included in the top category for each GO domain are shown in boxes. No GO categories were significantly enriched in the set of upregulated genes.

T24 cycle: n = 3, T7 cycle: n = 4 replicates; SCN tissue was pooled from 3 mice per replicate.

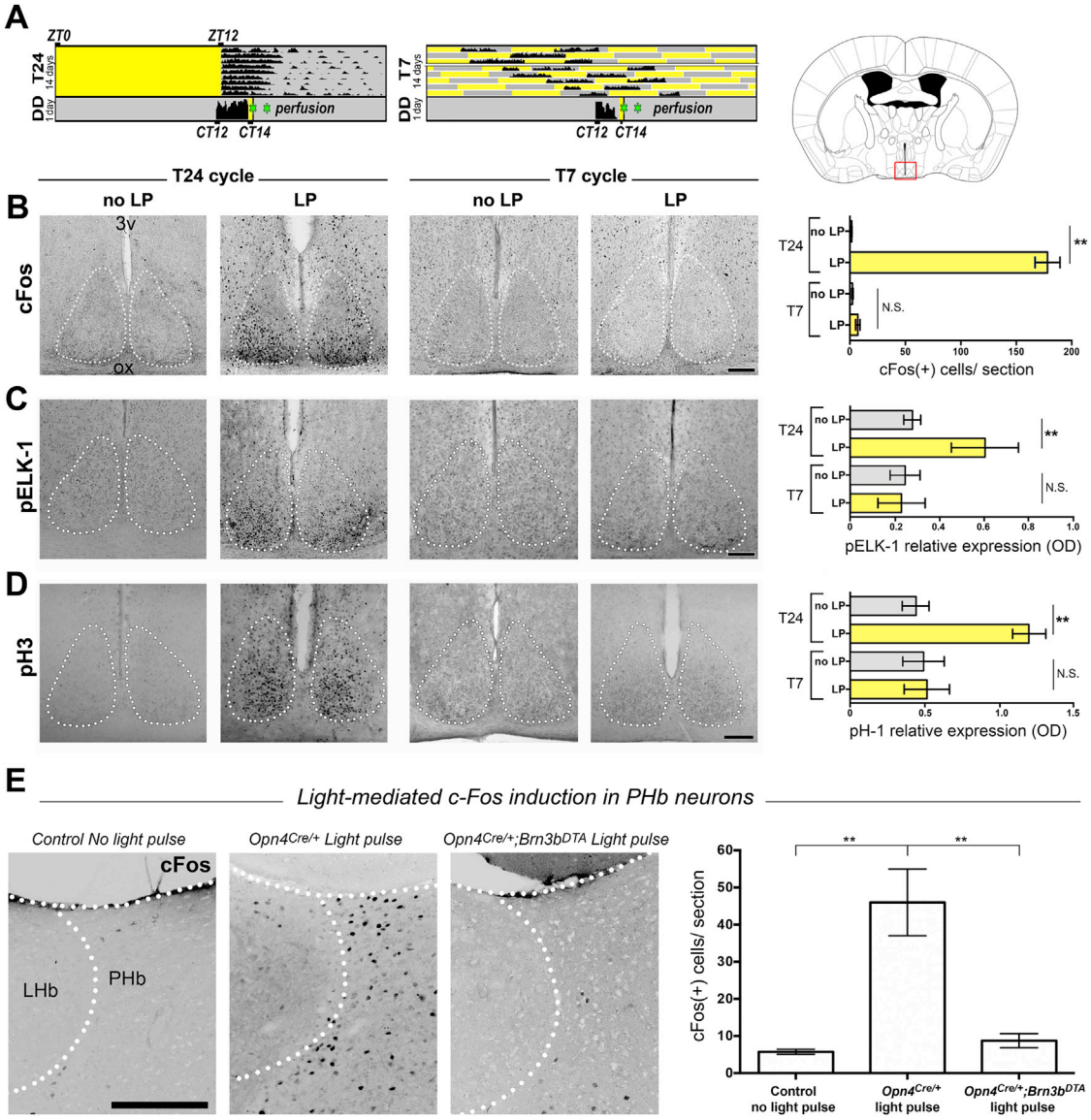


Figure S3. Light Responsiveness in the SCN and PHb, Related to Figures 2 and 4

(A) T24 and T7 cycle-housed WT mice were kept in darkness for 1 day, and received a light pulse (15 min) at CT14. For cFos analysis, after the light pulse mice were kept in darkness for 90 min, and perfused. For measuring phosphorylation of ELK-1 and H3, mice were perfused immediately after the light pulse.

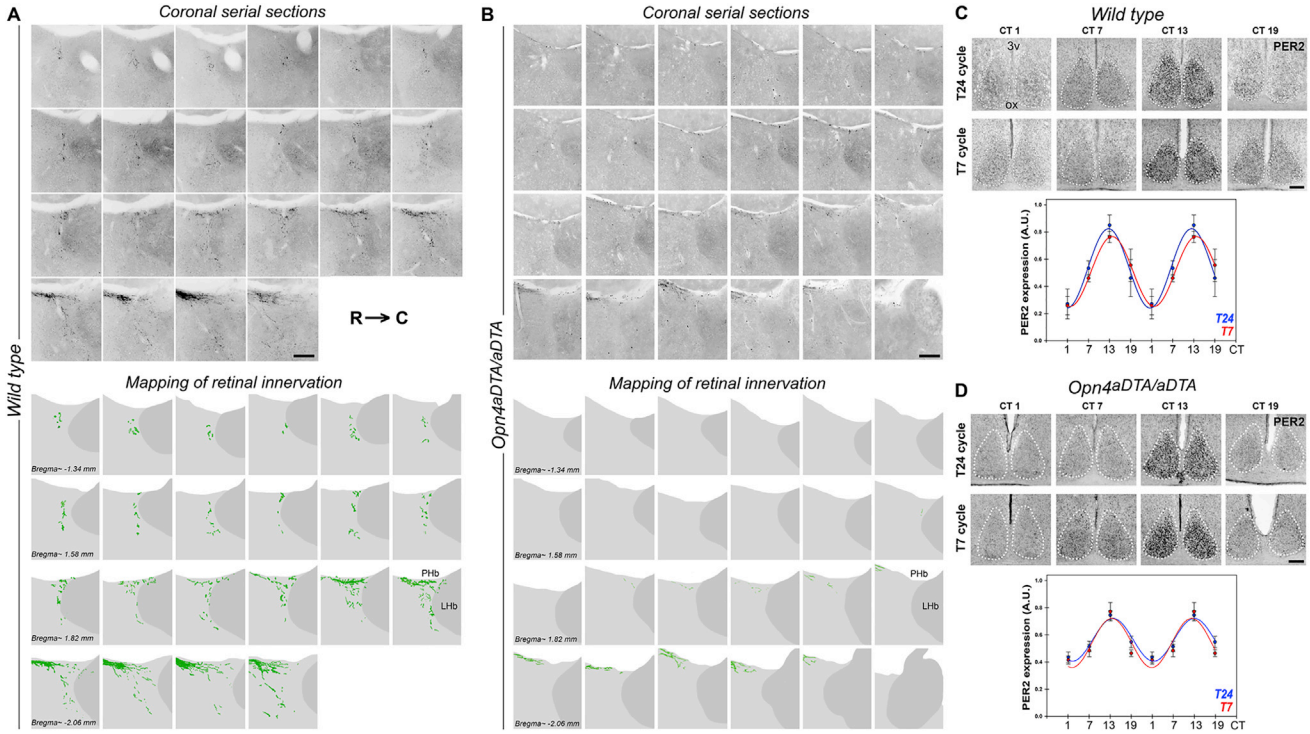
(B-D) A significant reduction in cFos induction (B), and in the phosphorylation levels of both ELK-1 (C) and H3 (D) were observed in T7 cycle-housed mice, compared to T24-housed mice. n = 5-6 mice.

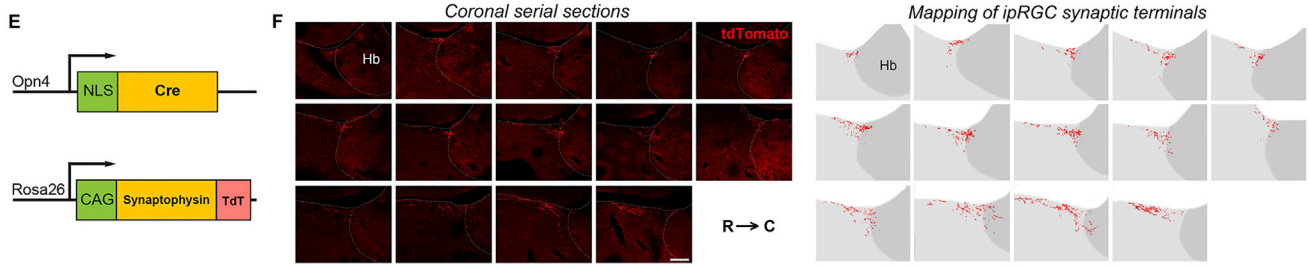
(E) Light-mediated c-Fos induction in the PHb. *Opn4*$^{Cre/+}$;*Brn3b*^{DTA} mice showed no significant induction of c-Fos in PHb neurons, compared to control (*Opn4*$^{Cre/+}$) mice. n = 3-4 mice.

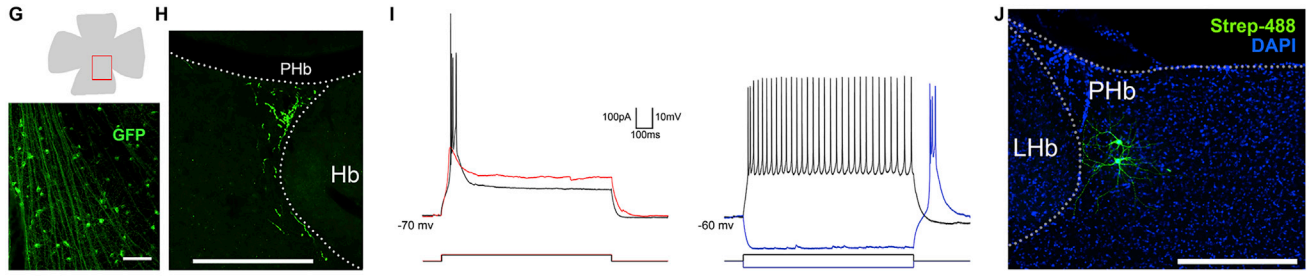
Data are mean ± SEM. **p<0.01, by Tukey's test.

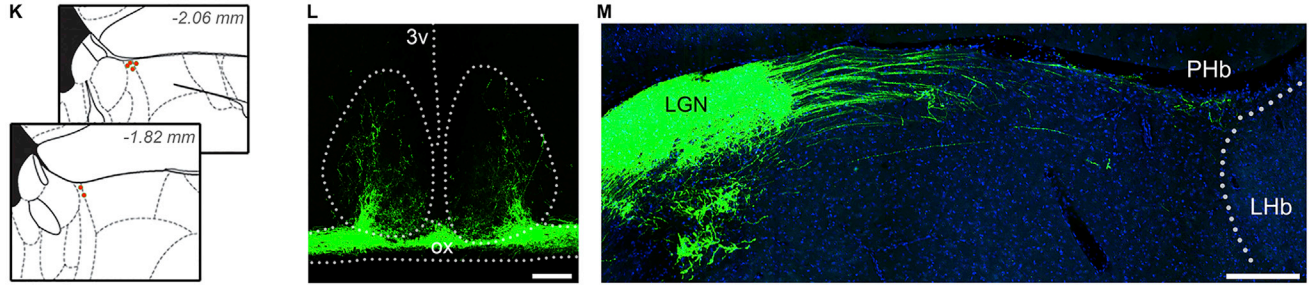
DD: constant darkness; ZT: *Zeitgeber* time; no LP: no light pulse; LP: light pulse. 3v, third ventricle; ox, optic chiasm.

Scale bars: (B, C, D) 100 μm, (E) 200 μm.









(legend on next page)

Figure S4. Retinal Input to PHb, Related to Figure 4

(A-B) CTβ was intravitreally injected in WT (A) and *Opn4*$^{aDTA/aDTA}$ (B) mice in order to trace retinal fibers. A complete serial sectioning of the PHb region and a reconstruction of retinal innervation (green) is also shown. In WT mice, a dense retinal innervation was observed throughout the PHb region of the dorsal thalamus. Mice lacking ipRGC innervation showed a drastic reduction in retinal innervation in the PHb. Four adult male mice were used to characterize the pattern of retinal projections.

(C-D) The rhythmic expression of the clock gene PER2 in SCN neurons was unaffected after the T7 cycle exposure in both control (C) and *Opn4*$^{aDTA/aDTA}$ (D) mice. Data are mean ± SEM, by Student's t test.

(E-F) A schematic representation of the mouse genetic lines used is shown (E). *Opn4*^{CreERT} mice were crossed with *ROSA*$^{Synaptophysin\text{-}tdTomato}$ mice. Finally, *Opn4*^{CreERT};*ROSA*$^{Synaptophysin\text{-}tdTomato}$ mice were used to study the pattern of ipRGC presynaptic terminals. tdTomato puncta expression was observed throughout the PHb region (F). A reconstruction of ipRGC presynaptic terminals (F, red) is also shown. Four adult mice were used to characterize the pattern of retinal projections and synaptic connectivity.

(G-H) An AAV2/ChR2-YFP was intravitrally injected (G), and retinal fibers GFP(+) were observed in the PHb (H).

(I) Electrophysiological characterization of PHb neurons. Cells were recorded in whole-cell current-clamp mode at two holding potentials. *Left panel:* When relatively hyperpolarized (−70mV), cells showed a burst mode of firing responses to depolarizing rectangular current pulses (black trace). Red trace represents the same cell after the application of TTX; note that the action potentials disappeared, but a depolarizing waveform persisted, known as the low threshold spike (LTS). This inward Ca^{2+} current, known as I_T, involves voltage- (and time-) dependent T-type Ca^{2+} channels and usually reaches the threshold for activating Na^+/K^+ action potentials, producing a brief burst of firing. *Right panel:* cells were then relatively depolarized (−60mV), I_T is inactivated, and a tonic mode of firing was observed in response to depolarizing steps (black trace). A hyperpolarizing current injection de-inactivates I_T and evoked a rebound burst response (blue trace). (n = 45 cells).

(J) Representative image showing two filled cells in the PHb region.

(K) A map showing the location of PHb neurons that displayed a response to ChR2 stimulation is shown.

(L-M) Adeno-associated viruses have been shown to be extremely efficient for inducing stable and prolonged expression of genes of interest in the retina. Among the broad variety of AAVs described to induce gene expression in many retinal cells after sub-retinal or intravitreal injections, AAV2 constitutes the most reliable option for infecting retinal ganglion cells (RGCs). When AAV2/ChR2-EYFP was intravitreally injected in WT mice, a strong gene induction (YFP) was observed in most RGCs. However, AAV2/ChR2-EYFP only infected a faction of ipRGCs, as reflected in most of their brain targets, including the SCN (L). Note the dense retinal innervation to LGN in (M). In AAV2/ChR2-EYFP injected mice that were also injected with the tracer CTβ, a quantification analysis revealed that only a fraction of axons colocalized for both markers (SCN: 23.5 ± 8.7%, PHb: 16.3 ± 9.8%, n = 3 mice). In sum, these results indicate that ipRGCs are particularly resistant to AAV infections, suggesting that the number of responder cells found in the PHb region could be underestimated due to the reduced infectivity of ipRGCs.

Hb: habenula; R: rostral; C: caudal; ox: optic chiasm; 3v: third ventricle,.

Scale bars: (C, D, G, L) 100 μm; (A, B, F, H, J, M) 200 μm.

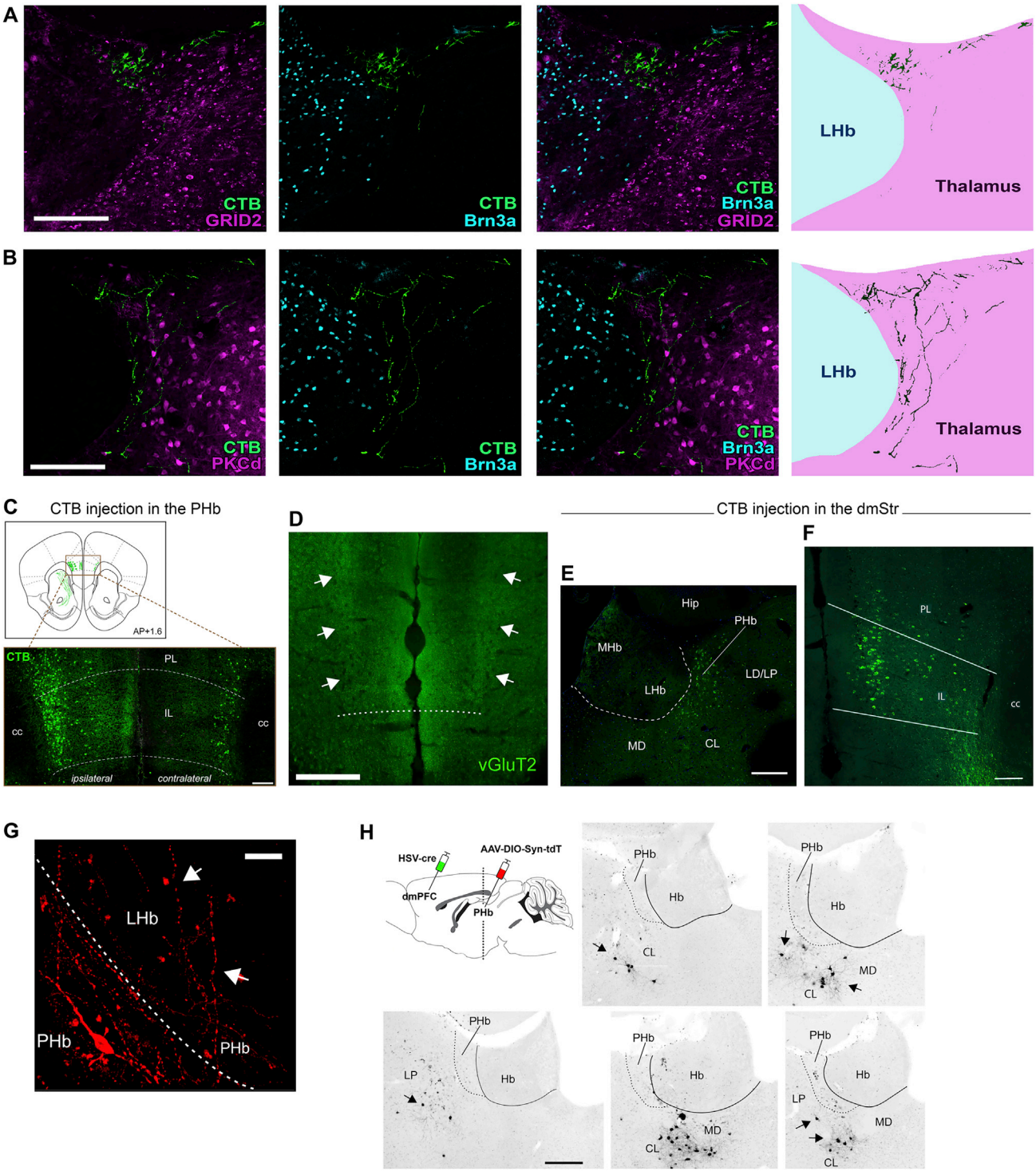


Figure S5. Thalamic PHb Projections to Brain Targets, Related to Figure 5

(A-B) Retinal fibers (CTβ) were observed in close apposition with thalamic neurons that express GRID2 (A) or PKCd (B).

(C) CTβ was injected into the PHb, and retrogradely labeled somas were clustered in layers V and VI of the IL and PL, bilaterally with respect to the injection site in the PHb; anterogradely labeled axons were evident in the IL ipsilaterally.

(D) vGluT2 staining was used to reveal the ventral boundary (dashed line) of the cortex. The ventral boundary of the cortex is pinpointed on the basis of striped vGluT2 expression pattern (arrows).

(legend continued on next page)

(E-F) CTβ was injected into the dorsomedial striatum (dmSrt) to determine, by retrograde tracing, the afferents of this PHb target (E). Labeled somas are also present in layers III-IV of the IL and PL, with sparse cells in layer V as well (F).

(G) Using the origin-controlled conditional tracing of the PHb downstream circuitry described, we found that a subset of labeled PHb neurons have collaterals penetrating into the lateral habenula (arrows).

(H) The PHb does not project to the dmPFC, unlike surrounding thalamic nuclei. HSV-cre was injected into the dorsal mPFC (specifically, in the anterior cingulate), while AAV-DIO-synaptophysin-tdTomato was injected into the PHb region (n = 3 mice). Sparse tdTomato+ somas were present mostly in the CL, with scattered neurons in the MD and rostromedial LP nuclei.

cc: corpus callosum; CL: centrolateral nucleus; MD: mediodorsal nucleus; PVT: paraventricular nucleus of the thalamus; Hb: habenula; dmPFC: dorsomedial prefrontal cortex.

Scale bar: (G) 25 μm; (A, B, C, E, F, H) 100 μm; (D) 200 μm.

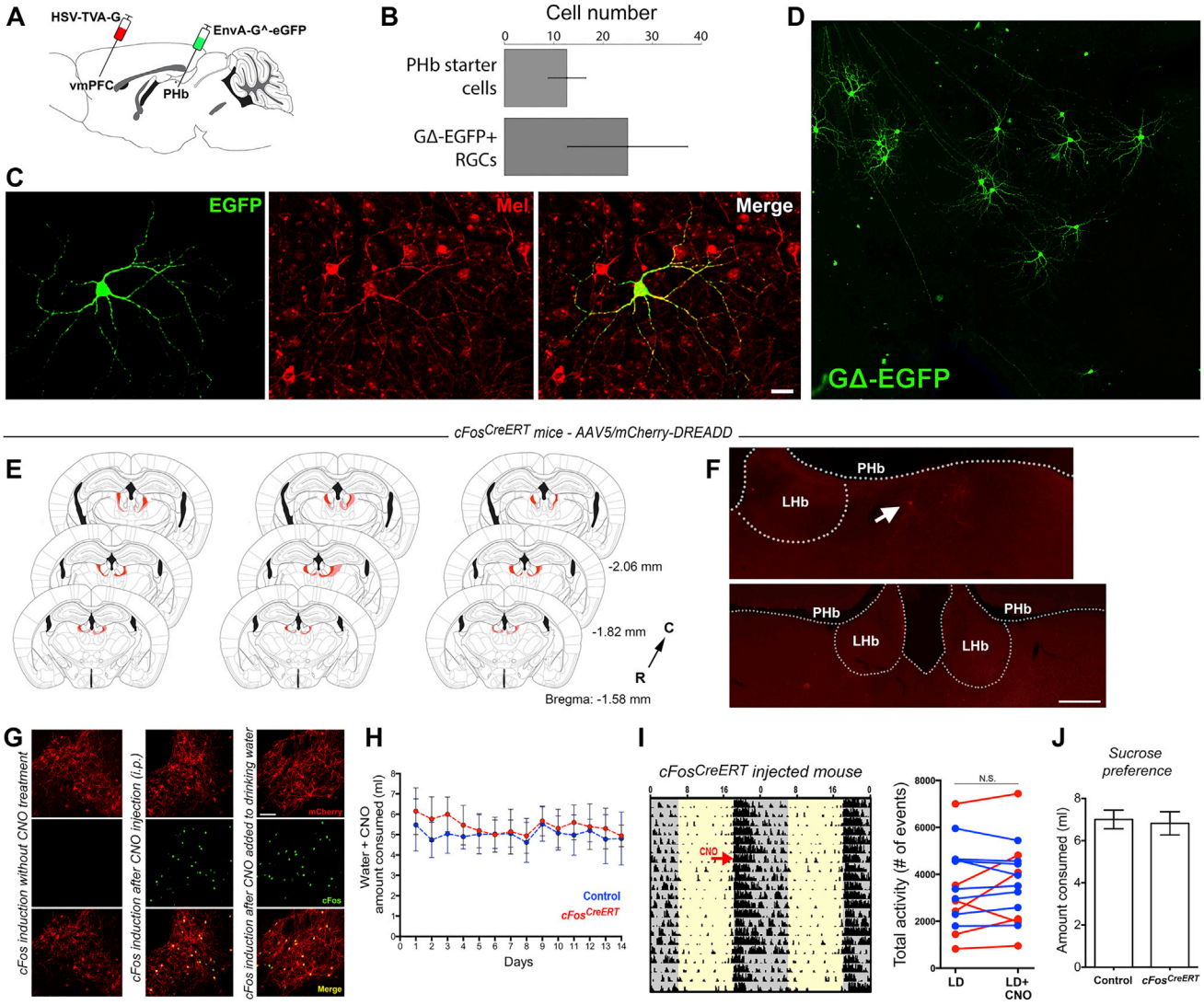


Figure S6. ipRGCs-PHb-vmPFC Pathway Drives Mood Alterations, Related to Figure 6

(A-D) A two-virus retrograde transsynaptic tracing system was used to identify RGCs feeding the retino-PHb-mPFC pathway. A retrograde helper vector (HSV-TVA-rabiesG-mCherry) was injected into the vmPFC, while EnvA-GΔRabies-EGFP was injected into the PHb (A). Only neurons transfected with the helper virus, and their immediate presynaptic neurons, can be infected by the rabies virus. The number of GΔRabies-EGFP+ starter neurons and ipRGCs found is shown (B, n = 3 mice). C-D: Retrolabeled RGCs (green) in the retina are predominantly melanopsin-immunoreactive (red).

(E) *cFos*^{CreERT2} mice were bilaterally injected in the PHb region with an AAV5/DIO-hM3D-mCherry. At the end of the behavioral tests, injection sites were evaluated. Schemes of coronal brain sections for three representative injected-mice are shown. Dark red areas represent regions of dense number of mCherry(+) cells; whereas light red regions represent areas with lower number of stained cells.

(F) *cFos*^{CreERT2} injected-mice exposed to the same protocol, but without light pulse exposure, showed only sparse (arrow, upper panel) or non mCherry(+) cells (lower panel) in the PHb region (n = 3 mice).

(G) The effects of clozapine-N-oxide (CNO) added to the drinking water were first compared with intraperitoneal (i.p.) CNO injections in WT mice stereotaxically injected with a Cre-dependent AAV encoding an excitatory(Gq). c-Fos induction was observed in most infected neurons in mice that received CNO in the drinking water (5 μg/ml), similar to results obtained from mice that received i.p. CNO injections (1mg/kg). Number of c-Fos(+) cells/ PHb section: Control: 0.4 ± 0.2; CNO (i.p.) injection: 56.3 ± 13.9; CNO in drinking water: 48.8 ± 15.3; data are mean ± SEM n = 3 mice.

(H) The daily consumption of water+CNO was evaluated in *cFos*^{CreERT} mice, and no differences were observed throughout the experiment, and compared with control mice. n = 8-12 mice.

(I) The locomotor activity was monitored using infrared sensors in mice housed under the T24 cycle. A representative actogram is shown; red arrow indicates the first day of CNO treatment. No significant alterations in the photoentrainment to a 12:12 hr light/dark cycle were observed (% activity during dark (active) phase: *cFos*^{CreERT}-injected mice = 97.3 ± 2.1; Control-injected mice = 96.5 ± 3.6). The total locomotor activity of mice was not affected by the CNO treatment, as observed in *cFos*^{CreERT}-injected (red) and control-injected (blue) mice.

(J) During the SPT, the total amounts consumed (water + sucrose) were comparable between groups.

Data are mean ± SEM, by Student's t test.

Scale bar: (C) 25 μm; (G) 50 μm; (D) 100 μm; (F) 200 μm.

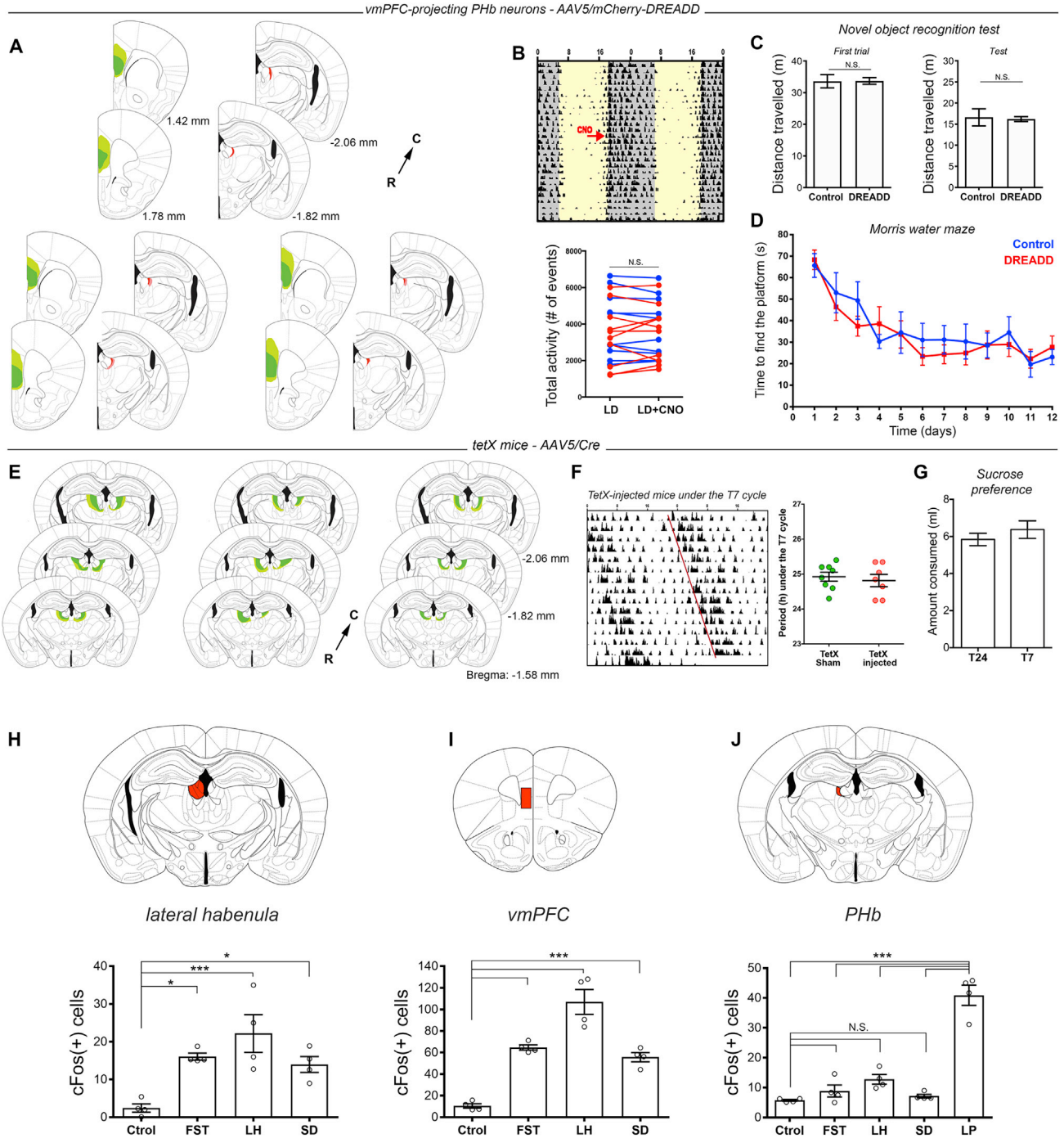


Figure S7. PHb Neuronal Function Has a Direct Impact on Light-Induced Mood Deficits, Related to Figure 7

(A) vmPFC-projecting PHb neurons were chronically activated using DREADD control. WT mice were bilaterally injected in the vmPFC with a retrogradely transported AAV1/cre and in the PHb region with an AAV5/DIO-hM3D-mCherry. At the end of the behavioral tests, injection sites were evaluated. Schemes of coronal brain sections for three representative injected-mice are shown. Dark green and red areas represent regions of dense number of GFP(+) or mCherry(+) cells, respectively; whereas light green and red regions represent areas with lower number of stained cells.

(B) The locomotor activity was monitored in T24 cycle-housed mice. A representative actogram is shown; red arrow indicates the first day of CNO treatment. No significant alterations in the photoentrainment to a 12:12 hr light/dark cycle were observed. The total locomotor activity of mice was not affected by the CNO treatment (% activity during dark (active) phase: AAV-injected mice = 92.6 ± 4.5; control-injected mice = 90.3 ± 4.2). Data are mean ± SEM, by Student's t test.

(C) Total distance traveled during the NOR test (*First trial*: familiarization session, mice have 10 min to freely explore two similar objects; *test*: 5 min exploratory time, where one of the objects was replaced by a novel object. n = 12-14 mice. Data are mean ± SEM, by Student's t test.

(legend continued on next page)

(D) Results obtained during the learning phase (12 days) of the MWM. Data are mean ± SEM n = 12-14 mice.
(E) Mice expressing tetanus toxin (tetX) in a Cre-dependent manner were bilaterally injected in the PHb region with an AAV5/Cre-GFP. At the end of the behavioral tests, injection sites were evaluated. Schemes of coronal brain sections for three representative injected-mice are shown. Dark green areas represent regions of dense number of GFP(+) cells, whereas light green regions represent areas with lower number of stained cells.
(F) tetX-injected mice were exposed to the T7 cycle, and the daily locomotor activity was monitored using infrared sensors. Under the T7 cycle, tetX-injected mice showed period lengthening, similar to T7 cycle-housed control (sham) mice. Data are mean ± SEM, by Student's t test. n = 14-15 mice.
(G) During the SPT, the total amounts consumed (water+sucrose) by tetX-injected mice housed under the T24 or T7 cycles were comparable. Data are mean ± SEM, by Student's t test.
(H-J) WT mice were exposed to a repeated forced-swim (FST), learned helplessness (LH), or chronic social defeat (SD) paradigms, and the induction of c-Fos was evaluated in the lateral habenula, vmPFC, and PHb. In all cases, stimuli were applied during the active phase of mice (∼CT 14), and during the sessions mice were kept in constant darkness to avoid any light-mediated effect on c-Fos induction. FST, LH and SD paradigms induced a significant increase in the number of c-Fos(+) cells in the lateral habenula (H) and vmPFC (I), whereas no significant induction of c-Fos was observed in PHb neurons (J), compared with control mice. Finally, we also found a significant difference in the effect of light pulse activation on PHb neurons, compared with all the paradigms used (J). Data are mean ± SEM, *$p<0.05$, **$p<0.01$, ***$p<0.001$, by Dunnett test. n = 4 mice.